Remote Sensing of Environment 232 (2019) 111324

Contents lists available at ScienceDirect

Remote Sensing of Environment

journal homepage: www.elsevier.com/locate/rse

Mapping fractional cover of major fuel type components across Alaskan tundra

Jiaying He[a,*], Tatiana V. Loboda[a], Liza Jenkins[b], Dong Chen[a]

[a] Department of Geographical Sciences, University of Maryland, College Park, MD, USA
[b] Michigan Technological Research Institute, Michigan Technological University, Ann Arbor, MI, USA

ARTICLE INFO

Edited by: Emilio Chuvieco

Keywords:
Alaskan tundra
Fuel type component
Wildland fire
Remote sensing
Landsat

ABSTRACT

Wildland fire is common and widespread in Alaskan tundra. Tundra fires exert considerable influence on local ecosystem functioning and contribute to climate change through biogeochemical (e.g. carbon cycle) and biogeophysical (e.g. albedo) effects. These treeless landscapes are characterized by a high degree of variation in fuel loading at scales much finer than moderate (30 m) satellite observations. However, because of the remoteness of the tundra and its lower contribution to carbon release compared to boreal forests, most frequently tundra fuels are poorly characterized, limiting the effective development of tundra-specific fire occurrence and behavior models. This study presents an approach to mapping the fractional coverages of major fuel type components in Alaskan tundra circa 2015 combining field data and Landsat 8 Operational Land Imager observations. We adopt a multi-step Random Forest method to estimate the fractional vegetation cover of woody, herbaceous, and nonvascular components at subpixel level. We demonstrate the strong capability of exploiting multi-seasonal spectral information to identify these component types, with R-squared values around 0.95 and root mean squared errors below 10% for predicting their fractional cover. Our mapping products depict the spatial distribution of woody, herbaceous, and nonvascular components at subpixel resolution across Alaskan tundra, which can function as a critical input for studying wildland fire risk and behavior in the tundra. The distributions of these fuel components align well with climate-based tundra ecoregions although climate variables are not included in our models.

1. Introduction

Wildland fire is common across tundra, the coldest vegetated land ecosystem on Earth. Active fire products derived from satellite data identify a widespread distribution of fire across the pan-Arctic tundra (Masrur et al., 2018). Out of the 10,260 km^2 global burned area in the tundra between 2001 and 2015, 54% was concentrated in Alaska as estimated by satellite-based burned area data (Loboda et al., 2017). Paleoecological and historical records also reveal frequent fire occurrence in Alaskan tundra (French et al., 2015; Higuera et al., 2011).

As a major disturbance in the tundra, wildfire exerts strong influence on the ecosystem state and functioning, including deepening of the active layer (Jones et al., 2015), release of ancient carbon to the atmosphere (Mack et al., 2011), decrease of land surface albedo (French et al., 2016) and shift in vegetation communities (Racine et al., 2004). These impacts further contribute to climate change through the alteration of surface energy budget and global carbon cycle (French et al., 2016; Mack et al., 2011; Pearson et al., 2013). Rapid climate warming in the Arctic observed during recent decades and projected under various climate change scenarios is likely to increase tundra fire occurrence in the future (French et al., 2015; Young et al., 2017).

Despite its importance for global biogeochemical and biogeophysical processes, tundra fire receives much less attention compared to fire in other ecosystems. Although the number of studies on tundra fire has grown considerably in recent years, they mainly focus on quantifying post-fire impacts (French et al., 2016; Loboda et al., 2013) or examining fire regimes (French et al., 2015; Rocha et al., 2012). Critical for accurate monitoring of fire potential and for assessing its ecological and climatic impacts, in-depth knowledge of fire ecology and improved modeling capability of fire occurrence are still lacking for the tundra. Current approaches primarily developed upon boreal forest fire studies are thus insufficient to establish improved modeling and predictive capability to assess the present and future tundra fire potential.

Wildfire occurrence is controlled through the interaction of fuel, weather, and topography (Pyne et al., 1996). Effective modeling of fire occurrence requires accurate characterization of these environmental

* Corresponding author.
E-mail address: hjy0608@terpmail.umd.edu (J. He).

https://doi.org/10.1016/j.rse.2019.111324
Received 25 January 2019; Received in revised form 14 July 2019; Accepted 15 July 2019

Table 1
LANDFIRE fuel products and their major fuel strata or types for Alaskan tundra.

Fuel classification system	Major fuel strata or types
13 Anderson Fire Behavior Fuel Model (FBFM13; Anderson, 1982)	Grass, shrub, timber, logging slash
40 Scott and Burgan Fire Behavior Fuel Model (FBFM40; Scott and Burgan, 2005)	Nonburnable, grass, grass-shrub, shrub, timber-understory, timber litter, slash-blowdown
Canadian Forest Fire Danger Rating System (CFFDRS; Hirsch, 1996)	Coniferous, deciduous, mixedwood, slash, open
Fuel Characteristic Classification System (FCCS; Ottmar et al., 2007)	Canopy, shrub, nonwoody fuels, woody fuels, litter-lichen-moss, ground fuels

factors. This is, however, difficult for the tundra under current efforts due to the lack of in situ data for all three factors. Compared to other ecosystems, very limited fuel inventory plots have been visited in Alaskan tundra because of its remoteness. Existing fuel type products provided by LANDFIRE (https://landfire.gov) for Alaskan tundra (Table 1) are primarily developed based on the generic fuel classification schemes designed for other ecosystems. In particular, FBFM13, FBFM40 and CFFDRS include logging slash in their schemes and thus cannot describe the surface fuel compositions in the tundra. Limited fire weather stations and little to none geodetic surveys within Alaskan tundra also lead to the lack of accurate weather and topographical measurements. Primarily built upon remotely sensed observations, models and interpolations, existing strategies and datasets developed for wildfire monitoring thus simply provide a generic estimation of the tundra environment in Alaska.

Whereas, tundra environment varies at a very fine spatial scale with extremely high local heterogeneity (Davidson et al., 2016; Frost et al., 2014; Lara et al., 2018; McManus et al., 2012), which makes existing products poorly suited for capturing its detailed spatial variability. Specifically, Alaskan tundra presents a highly variable and mixed combination of burnable vegetation materials, including shrubs, herbaceous plants, mosses and lichens. These fuel type components can affect fire occurrence and behavior in multiple ways (Innes, 2013; Rocha et al., 2012). First, fuel flammability varies by plant types in Alaskan tundra (Sylvester and Wein, 1981). Live leaves from shrub species tend to have higher fire-potential ratings than herbaceous plants. Second, the variability of post-fire fuel recovery and accumulation rates among vegetation types can lead to different fire frequency levels across the tundra (Innes, 2013). Tundra regions dominated by grasses or sedges tend to burn more frequently than those with shrubs or mosses do because of their faster recovery rates. Third, tundra vegetation composition also impacts burned area extent (Rocha et al., 2012). For example, larger burned areas are more frequently found within moist shrub and tussock tundra compared to non-acidic tundra. Thus, identifying the detailed composition and distribution of fuel type components is critical for understanding tundra fire occurrence and behavior.

However, the fine-scale fuel components in the tundra can only be separated at centimeter-level resolution with drone data (Fig. 1) and are not directly classifiable even in very high resolution (VHR; 1–5 m) imagery. Categorical LANDFIRE products developed at 30-m resolution poorly capture the actual fuel distribution in the tundra. Recent efforts, although limited, have been conducted to characterize the fractional vegetation properties at subpixel level for Alaskan tundra with Landsat imagery. For example, Macander et al. (2017) developed fractional coverage maps of plant functional types (PFTs) across the North Slope region of Alaska. Berner et al. (2018) also mapped the fractional dominance and aboveground biomass (AGB) of shrubs on the North Slope. However, these products are not directly transferable to fuel classification schemes in the tundra because of the different vegetation cover definitions adopted. They also fail to capture the information of other tundra regions like Seward Peninsular and Noatak, which have more frequent and intense fire activities than the North Slope based on historical records (French et al., 2015; Rocha et al., 2012).

While fractional cover products for tundra are only at their early stages of emergence, a variety of approaches has been developed to unmix land cover fractions with multi-source remote sensing data across different (most frequently tree dominated) ecosystems. Supervised regression algorithms with multi-temporal spectral metrics are among the most commonly adopted methods for fractional cover mapping (Hansen et al., 2013; Olthof and Fraser, 2007; Selkowitz, 2010). Random forest (RF) regression, an ensemble learning method based on decision tree regression, has been found to have strong capability in distinguishing vegetation fractions (Gessner et al., 2013; Liu et al., 2017; Marino et al., 2016). A second type of algorithms employs spectral mixture analysis to decompose sub-pixel fractional coverages (Guan et al., 2012; Ma et al., 2015; Mu et al., 2018; Okin, 2007). They primarily rely on spectral indices to determine the fractions of endmembers. However, the variability among endmembers is typically ignored in the modeling procedure (Somers et al., 2011). A third type of geometric-optical models has also been developed to derive vegetation fractions with multi-angular remote sensing data (Chopping et al., 2012, 2008), though their applications are limited by the spatial data coverage.

The NASA's Arctic-Boreal Vulnerability Experiment (ABoVE) has provided a new opportunity for conducting in-depth research on wildland fire in the tundra. Through the support of field campaigns by this program, researchers have been able to enlarge the spatial coverage and environmental conditions of field observations. Coupling with remote sensing datasets and existing algorithms, these field datasets make it possible to develop broad-scale mapping products for the tundra. In this study, we present an RF-based approach to mapping the fractional distributions of wildland fuel components in Alaskan tundra using multi-spectral and multi-temporal Landsat data circa 2015 and a suite of field observations collected across a large span of tussock and shrub tundra sites. Specifically, we focus on three fire-carrying fuel type components for the shrub or graminoid dominated tundra in our study area: 1) woody (shrub) component, 2) herbaceous (primarily sedge and grass) component, and 3) nonvascular (lichen and moss) component, and further develop separate maps for describing their fractional coverages. We determine these components in a qualitative way considering their differences in vegetation genera, fuel characteristics and spectral properties. This scheme also corresponds to fuel strata in FCCS and major fuel components in other existing systems (Table 1).

2. Study area

Our study area of Alaskan tundra was determined using the Circumpolar Arctic Vegetation Map (CAVM; Walker et al., 2005; Fig. 2), which has been widely applied in defining the tundra region in Alaska (Beck et al., 2011; Bhatt et al., 2013; French et al., 2015; Raynolds et al., 2008). Burning in Alaskan tundra is primarily supported by surface vegetation fuels including evergreen or deciduous shrubs, herbaceous species (sedges and grasses), mosses and lichens (Hu et al., 2015; Rocha et al., 2012). Dry sites in the tundra tend to be dominated by dwarf shrubs with some grasses, mosses, and lichens, while wet sites have more sedges and mosses (Sylvester and Wein, 1981).

Alaskan tundra shares similar vegetation communities and species across ecoregions (Alaska Department of Fish and Game, 2006; Viereck et al., 1992). The Unified Ecoregions of Alaska identifies four ecoregion groups and eleven ecoregion units within Alaskan tundra based on their climate, vegetation, geology, and topography (Nowacki et al., 2003;

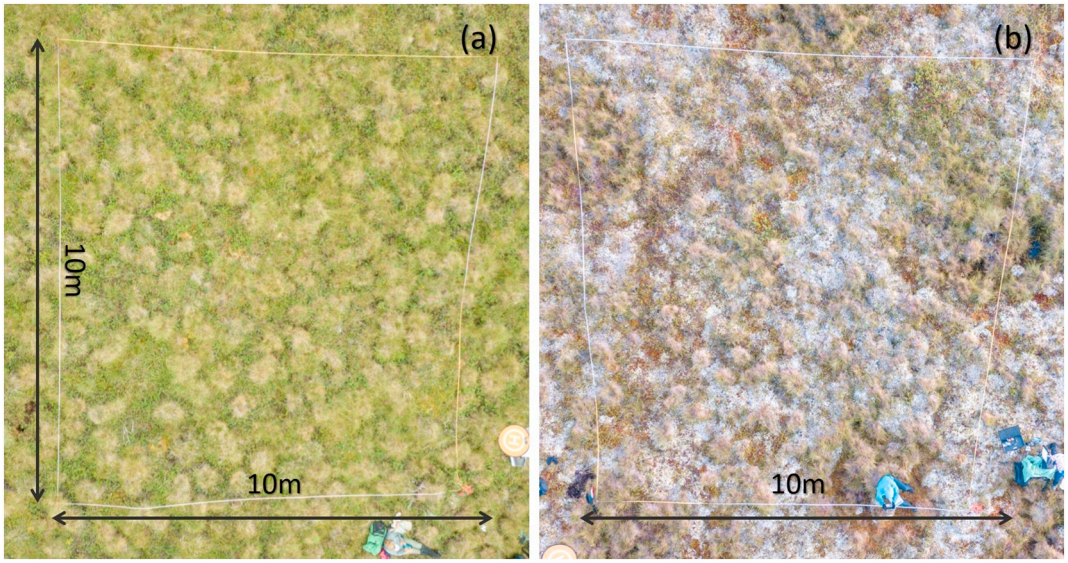

Fig. 1. Examples of highly mixed fuel components in Alaskan tundra: (a) shrub and graminoid tussocks; (b) grass, lichen and moss.

Fig. 2). With a dry, polar climate, the Arctic Tundra ecoregion group is dominated by shrub and sedge tundra underlain by continuous permafrost. The Bering Tundra group shows a moist polar or maritime climate with principally Dryas-lichen and moist sedge-tussock tundra. Bering Taiga group, having a moist polar climate with relatively thin permafrost, is generally covered by Dryas-lichen, sedge-shrub tundra and mixed forests. Dominated by a dry continental climate, the Intermontane Boreal group are primarily covered by shrublands and forests.

3. Data and methods

The variability of the tundra vegetation types in surface reflectance

Fig. 2. Alaskan tundra region defined by CAVM and corresponding ecoregions identified by the Unified Ecoregions of Alaska: 2001 (Nowacki et al., 2003). Each colour represents one ecoregion unit. Ecoregion units within the same Level 2 ecoregion groups are separated by different line patterns.

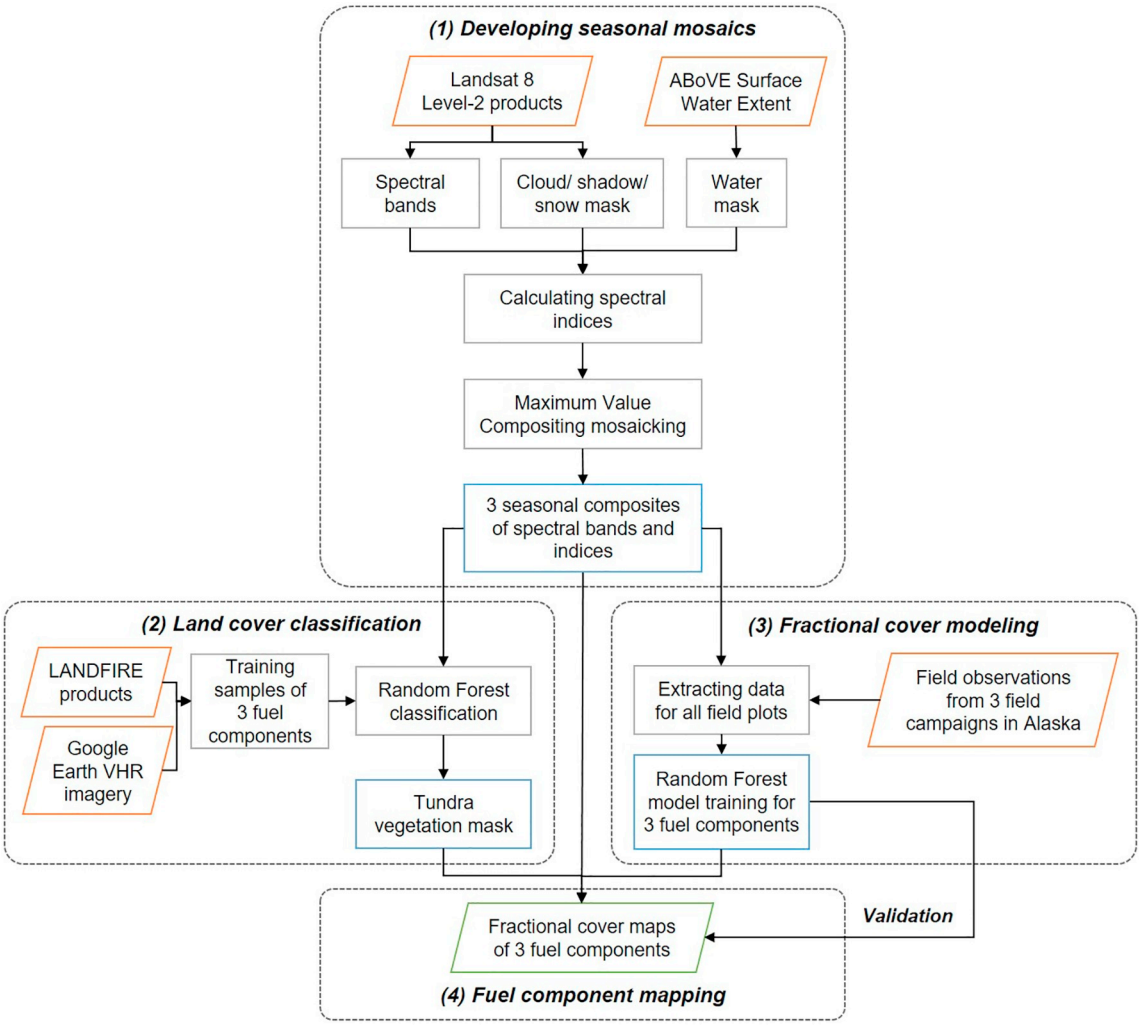

Fig. 3. Flowchart of fractional fuel components mapping.

and phenology makes it possible to capture the subpixel compositions using multi-spectral and multi-temporal remote sensing data. Dwarf shrub, sedge, and moss/lichen mix show distinguishable spectra according to the ground-based hyperspectral profiles measured in the North Slope (Buchhorn et al., 2013; Davidson et al., 2016). Both field observations and satellite-derived spectral indices also identify considerable variations in the phenology patterns of tundra vegetation species during their short growing seasons (Beamish et al., 2017; Shaver and Kummerow, 1991; Stow et al., 1993). For example, graminoid species such as tussock cottongrass (*Eriphorum vaginatum*) and Bigelow's sedge (*Carex bigelowii*) tend to have an earlier onset of leaf expansion compared to shrub species like tealeaf willow (*Salix pulchra*) and dwarf birch (*Betula nana*; Shaver and Kummerow, 1991). By summarizing the fuel properties, spectral characteristics and phenology patterns of these vegetation types described above, we identified the following components of surface fuel types in Alaskan tundra for large-scale mapping in this study: 1) woody (shrub), 2) herbaceous (primarily sedge and grass), and 3) nonvascular (lichen and moss).

We then designed a four-step method to map the spatial distributions of these fuel components (Fig. 3): (1) developing seasonal composites of spectral bands and indices with multi-temporal Landsat imagery for the entire Alaskan tundra (Section 3.2); (2) generating a "tundra vegetation mask" to identify the shrub or graminoid dominated tundra with land cover classification (Section 3.3); (3) RF modeling of fractional fuel component cover (Section 3.4); (4) mapping fractional cover of major fuel type components across the shrub or graminoid dominated tundra in Alaska (Section 3.5).

3.1. Data sources

3.1.1. Landsat data

Landsat 8 Operational Land Imager (OLI) imagery acquired from 2013 to 2017 was used to develop spatially continuous mosaics of Alaskan tundra. We downloaded the Level-2 surface reflectance data generated with Landsat 8 Surface Reflectance Code (LaSRC; Vermote et al., 2016) from USGS Earth Resources Observation and Science

Table 2
Summary of Landsat 8 OLI tiles processed in this study. WRS2 path/row overlaps exist between different regions.

Major regions	WRS2 path range	WRS2 row range	Total number of path/rows	Total number of scenes
North Slope and Noatak	64–85	10–13	70	932
Seward Peninsula	75–84	13–15	25	358
Southwest Alaska	73–80	15–19	29	752

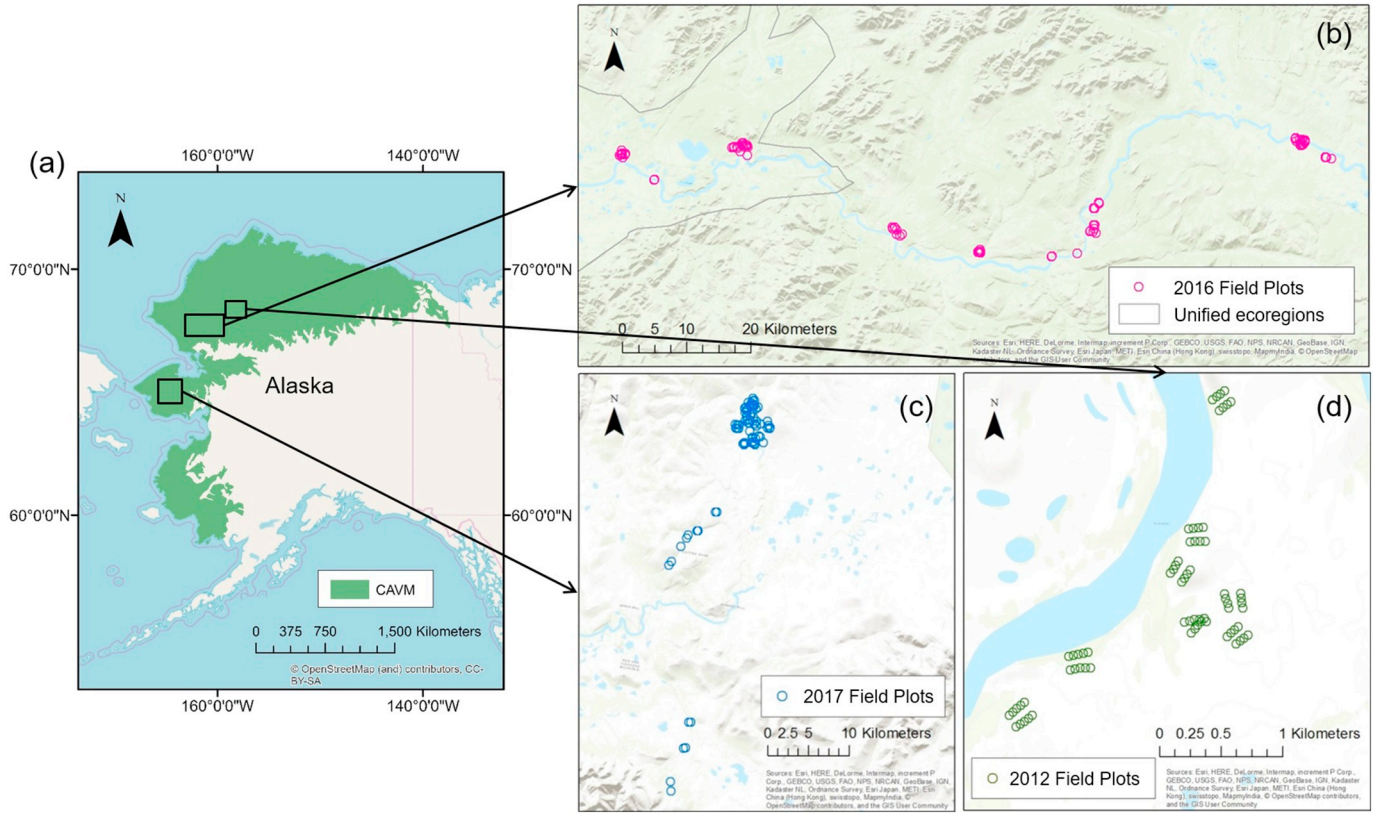

Fig. 4. Alaskan tundra region as defined by CAVM (a; Walker et al., 2005) and three field campaign sites: (b) 2016 field plots in Noatak River National Preserve, (c) 2017 field plots in Seward Peninsula, (d) 2012 field plots in North Slope.

Center (Table 2). Since the growing seasons of tundra vegetation generally start from late-April or May and end in October, for each year, we downloaded images acquired during late-April through October with land cloud coverage < 70%, as estimated by the product metadata. Additionally, we excluded images with 80–90% snow coverage over vegetated land surface in late April, May and October based on our visual interpretation during the data download. In total, we obtained and processed 1837 Landsat 8 scenes covering 113 Worldwide Reference System-2 (WRS2) path/rows as summarized in Table 2.

3.1.2. Field observations

We collected fractional cover observations of the three fuel components from 222 10 × 10 m plots during three field campaigns in the tussock and shrub tundra of Alaska (Fig. 4): 2012 campaign in the North Slope (NASA Terrestrial Ecology Grant NNX10AF41G), 2016 campaign in the Noatak River National Preserve and 2017 campaign in the Seward Peninsula (NASA Terrestrial Ecology Grant NNX15AT79A). Fractional coverages of fuel components within each plot were determined using ocular assessment. All three campaigns were conducted during late-July to mid-August. Considering the limited amount of field sites that we can visit during one single field trip, we combined field data from all three campaigns in this study to provide a robust sample collection for driving an ecosystem-wide mapping method.

Field plots were established following a generally accepted scheme (Dyrness and Norum, 1983; Viereck, 1979). During each campaign, we collected data within recovering burns as well as within areas that have not been identified as burned by either management records or satellite observations. This data collection design ensured that field data observations sampled a broad range of fire history and topographical features with varying compositions of woody, herbaceous, and non-vascular vegetation cover. The 2016 and 2017 data collection campaigns also ensured that a variety of drainage conditions was incorporated into the stratified sampling scheme. Specifically we identified four drainage categories based on slope and flow accumulation using a method proposed by Kasischke and Hoy (2012). We then randomly selected South-East corner point for the 10 × 10 m plots considering these factors prior to field visits. Although assessment of fractional cover during the 2012 field visit was conducted using the similar protocol, the site set up was more systematic in order to support a proper characterization of field sites for radar observations. In this case, corner points of 10 × 10 m plots were set up in two parallel transect lines 100 m apart within an area of visibly uniform conditions following a previously established field protocol in existing studies (Bourgeau-Chavez et al., 2007, 2013).

3.1.3. Auxiliary data

To assist the development of seasonal composites, we utilized the 16-day Moderate Resolution Imaging Spectroradiometer (MODIS) Vegetation Indices product (MOD13Q1 Version 6) available on Google Earth Engine from 2013 to 2017 to examine the phenology of tundra vegetation and to determine the growing season periods for Landsat data collection and processing. The Normalized Difference Vegetation Index (NDVI) data layer in MOD13Q1 was used for deriving phenology trends.

Although the quality assessment (QA) band provided by the Level-2 LaSRC product identifies water pixels for each scene, we adopted the 30-m ABoVE Surface Water Extent data (Carroll et al., 2016) centered in 2011 to identify the representative extent of water bodies across the study area for spatial and temporal consistency. Using Landsat imagery centered on 1991, 2001 and 2011, this product maps the distribution of surface water across the boreal and tundra regions in North America in these epochs (Carroll et al., 2016).

To develop the tundra vegetation mask in step 3, we utilized a set of 30-m LANDFIRE products and VHR imagery freely available on Google Earth to assist the sampling of training and validation datasets for land cover classification. We acquired the FCCS, CFFDRS and FBFM40

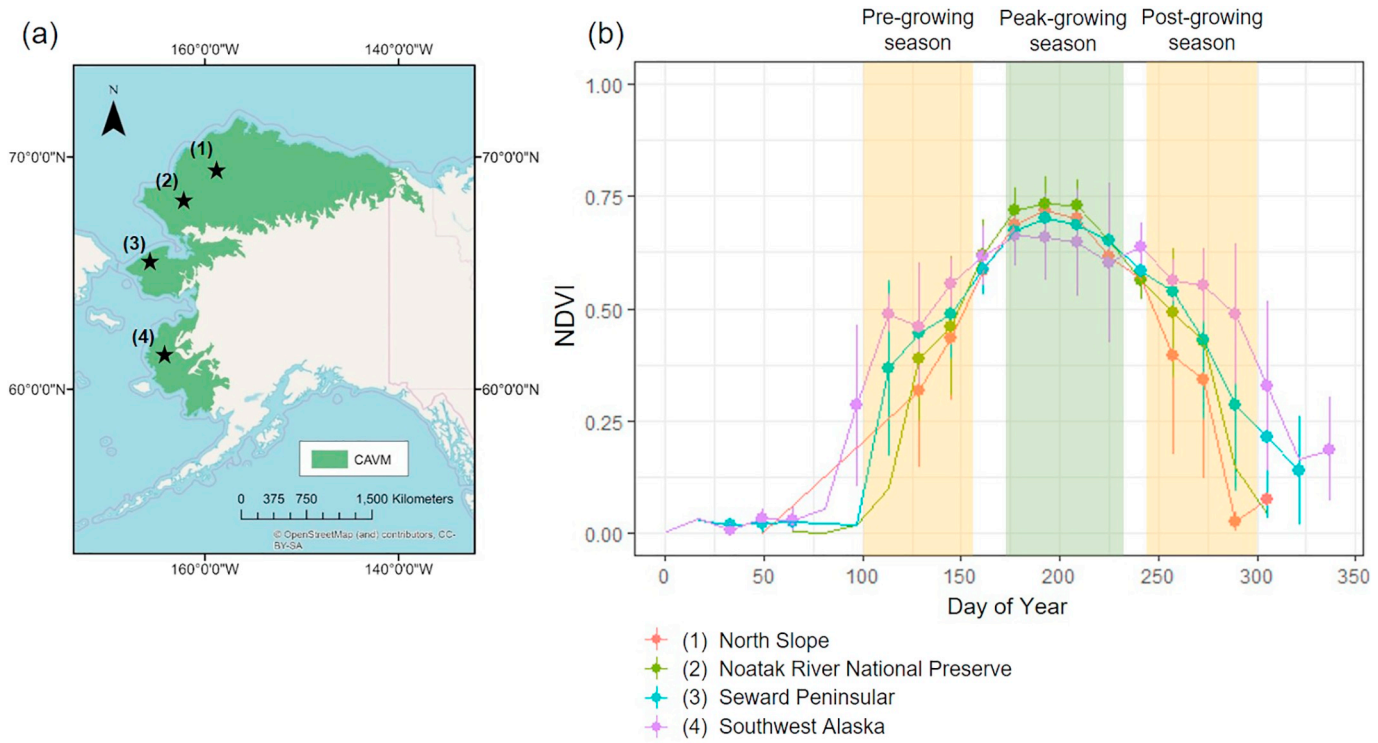

Fig. 5. Averaged NDVI profiles extracted from MODIS product (MOD13Q1) on Google Earth Engine in four regions across Alaskan tundra (a). Ten pixels were randomly selected and plotted for each region as an example (b): (1) North Slope, (2) Noatak River National Preserve, (3) Seward Peninsula, (4) Southwest Alaska.

products for Alaska (Table 1) in the latest available version 1.4.0, which incorporates Landsat imagery through 2014. VHR time series imagery provided by Google Earth was also accessed to help determine training and validation data through visual interpretation.

3.2. Developing seasonal composites of spectral bands and indices

First, we developed continuous composites of surface reflectance bands and spectral indices for pre-growing (late-April to early-June), peak-growing (mid-July to mid-August) and post-growing season (end-August to end-September). Since the specific timing of growing events varies by year and latitude, we extracted vegetation phenology patterns using NDVI data from MOD13Q1 to determine the specific dates of three growing seasons. We particularly examined four graminoid or shrub tundra regions as identified by CAVM across Alaska from north to south and compared the NDVI profiles of ten randomly sampled pixels in each region (Fig. 5). According to the vegetation growing patterns shown from the profiles, we assigned the Landsat data acquired from April 21 to June 10 as the pre-growing season, the data acquired from July 1 to August 20 as the peak-growing season, and the data acquired from August 30 to September 30 as the post-growing season.

We then downloaded and organized the Landsat 8 data by growing seasons, and extracted all surface reflectance and QA bands. Four ratio-based spectral indices and three Tasseled Cap (TC) components (Brightness, Greenness, and Wetness; Baig et al., 2014) were calculated for each scene to capture the detailed variability of vegetation spectral characteristics (Table 3). Particularly, we considered four ratio-based indices here including NDVI (Tucker, 1979), Normalized Burn Ratio (NBR; García and Caselles, 1991) Normalized Difference Water Index with near-infrared (NIR) and shortwave-infrared (SWIR) bands (NDWI1; Gao, 1996), and Normalized Difference Water Index with green and NIR bands (NDWI2; McFeeters, 1996).

Since Maximum Value Compositing (MVC) approach is effective in minimizing the impacts of cloud contamination, off-nadir viewing, aerosol and water vapor, we adopted this widely used method for developing seasonal mosaics across Alaskan tundra (Holben, 1986; Potapov et al., 2008; Roy et al., 2010; Stow et al., 2004). Before mosaicking, we masked out the cloud, cloud shadow, and snow pixels detected by the CFMask algorithm (Zhu et al., 2015). We further conducted morphological dilation for the masked pixels using a disk-shaped structuring element with five as the radius to remove the undetected cloud and shadow pixels. Although cloud/shadow pixels are generally thought to have lower NDVI than clear-sky pixels, pixels along the cloud/shadow edges mixed by shadow and vegetation signals could have higher NDVI than the clear-sky ones (Fig. 6). Since the dilated mask could still omit these edge pixels with high NDVI values that can affect MVC results, we further filtered them out using the following criteria based on empirical values identified in our study area:

$$\rho_{NIR} < 0.2 \; and \; NDVI > 0.6,$$

where ρ_{NIR} represents the surface reflectance of NIR band. For each growing season, we identified the Landsat pixels with the maximum NDVI and then generated the mosaics for each band using the values from these pixels. The three output mosaics each include six spectral bands and seven indices as listed in Table 3. They then served as the input data for the following steps.

3.3. Generating a tundra vegetation mask for shrub or graminoid dominated tundra

Since CAVM simply defines an approximate tundra boundary based on 1-km Advanced Very Higher Resolution Radiometer (AVHRR) data (Walker et al., 2005), we further developed a "tundra vegetation mask" layer to refine the shrub or graminoid dominated tundra region using RF classification. We have removed water body pixels in the previous step using the nominal water mask (Carroll et al., 2016). Here we identified three land cover classes including (1) tall shrub or tree, (2) built-up or barren land, (3) shrub or graminoid dominated tundra.

We first used the three acquired LANDFIRE products (CFFDRS, FBFM40 and FCCS) to define the general regions of the three classes

Table 3
Landsat 8 spectral metrics used for developing seasonal composites.

Categories	Properties	Details
Surface reflectance bands	Band 2	Blue: 0.45–0.51 μm
	Band 3	Green: 0.53–0.59 μm
	Band 4	Red: 0.64–0.67 μm
	Band 5	NIR: 0.85–0.88 μm
	Band 6	SWIR1: 1.57–1.65 μm
	Band 7	SWIR2: 2.11–2.29 μm
Ratio-based spectral indices	NDVI	$(\rho_{NIR} - \rho_{Red})/(\rho_{NIR} + \rho_{Red})$
	NBR	$(\rho_{NIR} - \rho_{SWIR2})/(\rho_{NIR} + \rho_{SWIR2})$
	NDWI1	$(\rho_{NIR} - \rho_{SWIR1})/(\rho_{NIR} + \rho_{SWIR1})$
	NDWI2	$(\rho_{Green} - \rho_{NIR})/(\rho_{Green} + \rho_{NIR})$
Tasseled cap components	TC brightness (TCB)	$0.3029\rho_{Blue} + 0.2786\rho_{Green} + 0.4733\rho_{Red} + 0.5599\rho_{NIR} + 0.508\rho_{SWIR1} + 0.1872\rho_{SWIR2}$
	TC greenness (TCG)	$-0.2941\rho_{Blue} - 0.243\rho_{Green} - 0.5424\rho_{Red} + 0.7276\rho_{NIR} + 0.0713\rho_{SWIR1} - 0.1608\rho_{SWIR2}$
	TC wetness (TCW)	$0.1511\rho_{Blue} + 0.1973\rho_{Green} + 0.3283\rho_{Red} + 0.3407\rho_{NIR} - 0.7117\rho_{SWIR1} - 0.4559\rho_{SWIR2}$

based on their classification codes (Table 4). We then examined the random points by visually interpreting the moderate resolution and VHR time series imagery available on Google Earth based on expert knowledge. Points that are not representative of the classes they are supposed to represent were removed from the sampling dataset. For each class, we extracted the intersections of each product as its boundary for generating stratified sample points by area. In total, we acquired 436 points for the tall shrub or tree, 1176 points for the built-up or barren land, and 5238 points for shrub and graminoid tundra.

We used all bands from the seasonal mosaics as the input features for training and mapping the tundra vegetation mask. For each class, we randomly selected 70% of the sampled points for training the RF classification algorithm and reserved the remaining 30% for assessing the classification accuracy. We also reported the overall out-of-bag (OOB) error rate to estimate the classifier error based on the training data. Specifically, the OOB error rate is generated by estimating the ratio of misclassification among all bootstrap iterations (Breiman, 2001).

3.4. RF modeling of fractional cover

Before modeling, we compared our designed sampling plots with our full fire records, including both MODIS Active Fire Product and Alaska Large Fire Database, to make sure that our plots were not impacted by fire and thus representative of undisturbed conditions since the time of the measurement. To predict the fractional cover of surface

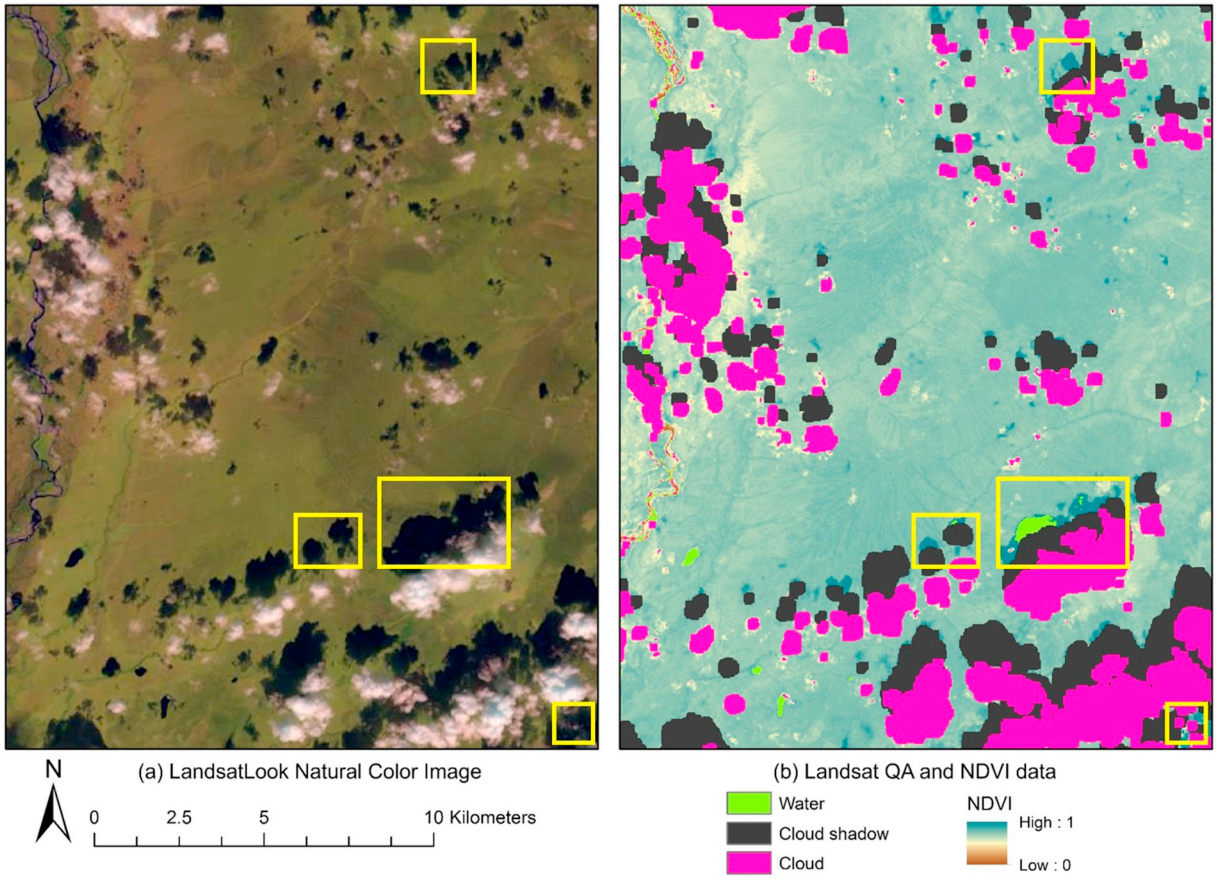

Fig. 6. Unmasked cloud shadow pixels with high NDVI values from a Landsat 8 scene (Landsat Scene Identifier: LC80690122017228LGN00) in our study area. Examples are highlighted in yellow rectangles: (a) LandsatLook natural colour image, (b) NDVI and cloud/shadow/water mask identified by Level-2 QA data from the same Landsat scene. (For interpretation of the references to colour in this figure legend, the reader is referred to the web version of this article.)

Table 4
Land cover classes and corresponding classification codes from LANDFIRE products.

Land cover classes	LANDFIRE products	Fuel class or identification code
Tall shrub or tree	FCCS	85, 87, 88, 89, 92, 93, 94, 101, 103, 105, 322, 332
	CFFDRS	C1, C2, C3, C4, C5, C6, C7
Built-up or barren land	FCCS	0
	CFFDRS	NB1, NB9
	FBFM40	NB1, NB9
Shrub or graminoid dominated tundra	FCCS	95, 97, 98, 99, 100, 318, 323, 324, 326, 327, 330, 331, 333, 334, 336, 337, 338, 339, 601, 602, 603, 604, 610, 611, 614, 615, 616, 617, 620, 623, 624, 625, 627, 629, 630, 632, 635, 637, 638
	CFFDRS	D1, S2, S3, O1A, M1, M2A, M2B, M2C, M3

fuel components at the large scale, we trained individual RF regression models for the three components separately with our field observations and seasonal composites developed in Section 3.2. In particular, the spectral properties from the three growing seasons, including all six surface reflectance bands, four ratio-based spectral indices, and three TC components, were used as the input parameters to train the RF models for estimating fractional cover. For each RF regression model, we set the number of input variables at each split to 14, the number of trees to grow as 500, and the node size to 5.

To assess the modeling accuracy, we not only examined the internal metrics provided by the RF regression algorithm, but also conducted cross-validation with our field observations. Specifically, we assessed the internal metrics including OOB, percent of variance explained, mean squared error (MSE) and root mean squared error (RMSE). For the cross-validation, we reserved 70% field data for model training and kept the remaining 30% for validation using a stratified random sampling strategy. We then reported the RMSE and R-squared values between the observed and estimated fraction values with the 30% validation dataset. For each fuel type component, we ran RF regression multiple times and selected an optimal one as the final model for estimating fractional cover.

We also assessed the importance of predictors in determining the fractional cover in each model. Although Mean Decrease Gini and Mean Decrease Accuracy (MDA; Breiman, 2001, 2002) are the most commonly used indicators to assess the contributions of independent variables; there is an on-going debate about their comparative robustness (Louppe et al., 2013). Here we chose to report the MDA, which evaluates the variable importance by estimating the mean decreased MSE with permutated variable values.

3.5. Fuel component mapping

In the final step, we combined the results generated from the previous sections to develop fractional cover maps for the three fuel components. Only shrub or graminoid dominated tundra pixels identified by the "tundra vegetation mask" in Section 3.3 were subsequently used for mapping. We used the RF regression models developed in Section 3.4 to estimate the fractional cover of fuel components in Alaskan tundra. In addition to the statistical metrics we have adopted for assessing the RF modeling accuracy in Section 3.4, we further assessed our mapping results through comparisons with existing data products at similar spatial scales considering the limited coverage of our field observations.

We first examined the distribution of our fuel component fractions against the ecoregions based on the expert knowledge. The variability of climatic and topographic conditions across ecoregions in the tundra affects the actual distribution of the burnable vegetation materials. Here we utilized the Unified Ecoregions of Alaska (Nowacki et al., 2003) product to define the ecoregions within the tundra (Fig. 2). For each fuel component, we generated boxplots to summarize the fraction distributions within the two Level 1 ecoregion groups ("Boreal" and "Polar"). Since most ecoregions in Alaskan tundra are elements of the "Polar" group, we further examined the distributions of each ecoregion units within the "Polar" Level 1 group.

We then compared our results with existing vegetation cover products developed for the North Slope of Alaska to examine the differences caused by fractional cover definitions, field sampling strategies, and modeling methods. Although no fractional fuel type products have been developed across Alaskan tundra, Beck et al. (2011) mapped the shrub cover of deciduous species circa 2000 and Macander et al. (2017) quantified the fractional distributions of 16 PFTs across the North Slope of Alaska. Here we examined these products against our field observations. We then compared the overall results between our maps and these two products with randomly selected sample points in the overlapping regions of all products. Since the definition of PFTs is not directly transferable to our fuel component scheme, here we used the "Total shrub" of PFT to compare with our woody component, the "Total herbaceous" of PFT to compare with the herbaceous component, and the "Total nonvascular plants" to compare with the nonvascular component. Although Berner et al. (2018) also mapped the dominance of shrub in the North Slope, they defined the shrub dominance differently as the percentage of shrub AGB over the total plant AGB and thus was not considered for comparison.

4. Results

4.1. Accuracy assessment of tundra vegetation mask

We used both internal metrics from the RF classification algorithm and accuracy assessment to evaluate the performance of our tundra vegetation mask. The RF algorithm showed an overall OOB error rate of 2.21%. We then generated the confusion matrix using the reserved 30% data to validate the classification result (Table 5). The overall classification accuracy reaches 97.91%, although the producer's accuracy and

Table 5
Confusion matrix of land cover classification for developing tundra vegetation mask.

		Reference				
		Tall shrub/tree	Built-up/barren	Tundra	Total	User's accuracy
Map	Tall shrub/tree	102	0	11	113	90.27%
	Built-up/barren	0	351	1	352	99.72%
	Tundra	29	2	1560	1591	98.05%
	Total	131	353	1572	2056	1
	Producer's accuracy	77.86%	99.43%	99.24%	1	Overall accuracy: 97.91%

Table 6
Statistical summary of three RF regression models.

Fuel component	% variance	MSE	RMSE
Woody component	79.83	0.008852	9.41%
Herbaceous component	80.76	0.008117	9.01%
Nonvascular component	80.02	0.007234	8.51%

user's accuracy vary among each land cover class. The class of tall shrub or tree receives the lowest producer's accuracy (77.86%) and user's accuracy (90.27%), while the other two classes have consistently high accuracy values. Across the 494,971.4 km^2 Alaskan tundra as estimated by CAVM, we identified 380,755.2 km^2 as shrub or graminoid dominated tundra.

4.2. Accuracy assessment of fractional cover estimation

To assess the modeling results, we first examined the internal metrics generated from RF regression (Table 6). The RF models developed for all three fuel components perform well in explaining the percent of the variance, with 79.83%, 80.76%, and 80.02% for the woody (shrub), herbaceous (sedge and grass), and nonvascular (lichen and moss) components respectively. They also report high predictive power for fractional cover mapping with low MSE and RMSE values. The woody, herbaceous and nonvascular models show MSE values of 0.008852, 0.008117 and 0.007234, and RMSE values of 9.41%, 9.01%, and 8.51%, respectively.

We then evaluated the predicted fractional cover using the reserved 30% field samples. The comparisons between the modeled and observed values show strong agreement for the three fuel components (Fig. 7). The RSME values for the validation samples are within 2% of those generated from the internal model statistics with 8.04%, 9.57%, and 10.11% for woody, herbaceous and nonvascular components, respectively. The R-squared values between observations and estimations for the validation data are approximately 0.95 for all fuel components, with 0.9717, 0.9633, and 0.9395 for the woody, herbaceous and nonvascular components respectively.

Spectral bands and indices during pre- and peak-growing seasons play the most important role in determining the fractional cover of woody and herbaceous components in Alaskan tundra (Fig. 8 a-b), while spectral indices during post-growing seasons contribute most to the cover estimation of nonvascular component (Fig. 8 c). For the woody component, the spectral reflectance of the red band during the peak-growing season shows the highest MDA value of 14.73% in the RF regression model, followed by that of the blue band during the pre-growing season (13.53%) and NDVI during the peak-growing season (11.78%). For the herbaceous component, the spectral reflectance of the red band during the pre-growing season shows the highest MDA value of 16.66%, followed by NBR during the peak-growing season (15.79%) and the spectral reflectance of the green band during the pre-growing season (13.83%). As for the nonvascular component, NBR during the post-growing season is the most important independent variable in the regression model with an MDA value of 19.15%. NDWI2 and NDVI during the post-growing season also show high MDA values (13.77% and 11.75% respectively) in determining the fractional cover. Although RF regression can alleviate the multicollinearity issue through bootstrap aggregation, biases in variable importance can still exist among correlated features.

4.3. Fractional cover of major fuel type components across Alaskan tundra

We mapped the fractional distributions of three fuel components across the shrub and graminoid tundra in Alaska circa 2015 (Fig. 9). From the south to the north of Alaska, shrub cover shows a slightly decreasing trend as the temperature falls (Fig. 9a). The Southwest Alaska shows a larger portion of the area with high shrub fraction compared to the North Slope and the Seward Peninsula. For the North Slope and the Seward Peninsula, shrub cover is higher along the rivers (Fig. 9). The herbaceous component of sedge and grass is dominant and widely distributed across the entire study area (Fig. 9b). In particular, the central North Slope has a high fractional cover of sedge and grass. As can be expected, the nonvascular component is highly concentrated in the northern part of the North Slope (Fig. 9c). From the north to the south across the entire tundra region, a general decreasing trend in the distribution of lichen and moss is clearly observed.

A closer examination of our mapping results in the Noatak River National Preserve shows an increase in the shrub fraction along the drainages (Fig. 10b), while other regions have higher coverages of the herbaceous fuels including sedge and grass (Fig. 10c). The amount of the nonvascular component is generally low in this example and is most frequently observed in high concentrations only close to the barren land along the river or the mountains (Fig. 10d).

We then summarized the spatial distributions of fractional fuel cover by the unified ecoregions (Nowacki et al., 2003) in Alaskan tundra to examine their patterns. As expected, the comparison between the two Level 1 schemes (Boreal and Polar) shows a higher coverage of the woody component within the “Boreal” scheme (Fig. 11a). The “Boreal” scheme has a mean shrub coverage of 37.96% while that of the “Polar” scheme has a lower mean value of 31.57%. The “Boreal”

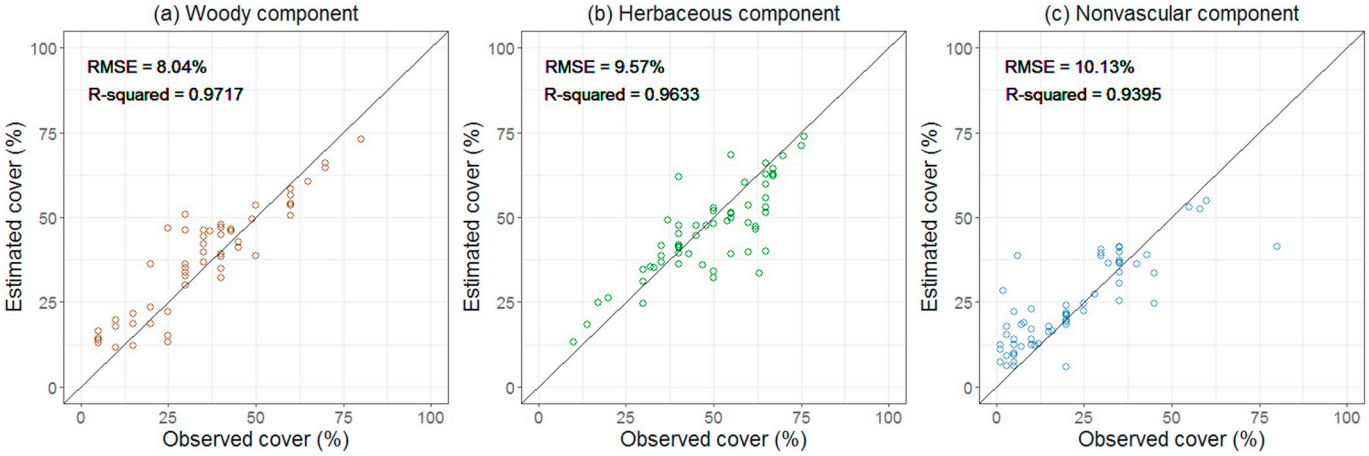

Fig. 7. Scatter plots comparing estimated and observed fractional cover using the validation data for (a) woody, (b) herbaceous, and (c) nonvascular components. RMSE and R-squared values between the estimations and observations are reported in the scatter plot of each component. RSMEs are within 2% of those from the internal model statistics. R-squared values reach 0.95 for all components.

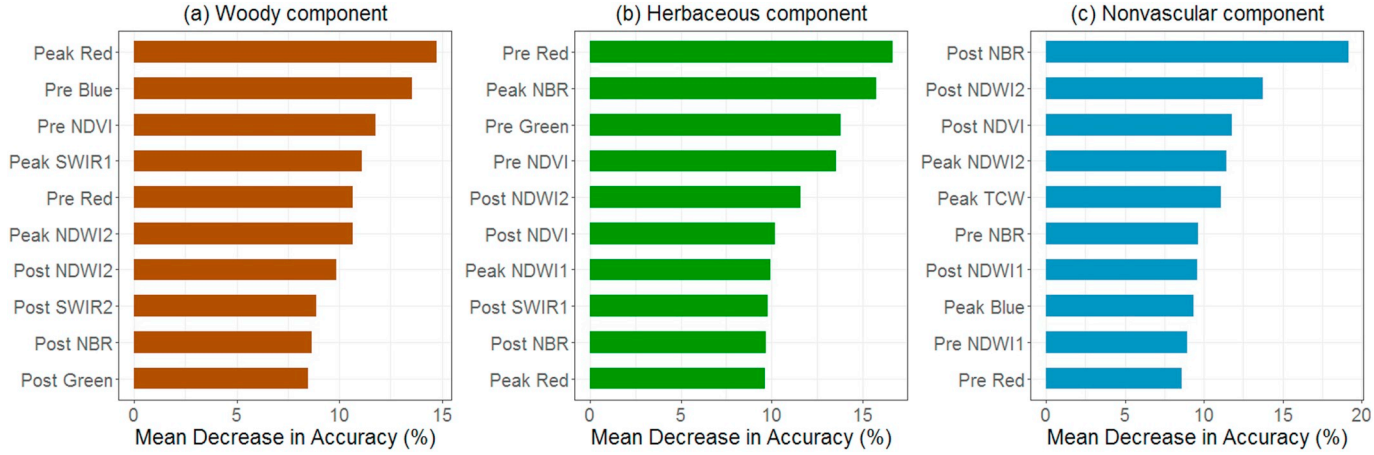

Fig. 8. Top 10 important independent variables and their MDA values from RF regression models for (a) woody, (b) herbaceous and (c) nonvascular components. Spectral bands and indices during pre- and peak-growing seasons play the most important role in determining the fractional cover of woody and herbaceous components (a-b), while spectral indices in the post-growing seasons contribute most to the cover estimation of nonvascular component (c).

scheme has an interquartile range (IQR) of 33.23% to 43.47%, while the IQR of "Polar" ranges from 24.23% to 37.82%. Since the "Polar" scheme includes three Level 2 groups and nine ecoregion units, we further examined the distribution of shrub coverage within this scheme. From north to south, the shrub coverage increases gradually among all the Level 2 groups and the ecoregion units (Fig. 11b). The woody component cover of units in "Arctic Tundra" and "Bering Tundra" is comparable but lower than that in the "Bering Taiga" in general. Specifically, the "Beaufort Coastal Plain" located in the northernmost part of Alaska has the lowest shrub cover on average of about 27.61%, while the southernmost "Ahklun Mountains" unit has the highest mean cover of about 39.04%.

For the herbaceous component (sedge and grass), the comparison between the two Level 1 schemes (Boreal and Polar) suggests no obvious differences (Fig. 12a). The "Boreal" scheme shows a mean herbaceous coverage of 38.76% while that of the "Polar" scheme has a higher value of 39.58%. The IQR of "Boreal" and "Polar" schemes are about 33.77%–43.23% and 33.28%–45.68% respectively. The mean fractional cover values of all Level 2 groups are also comparable in general, with values of about 38% to 40%. The sedge/grass distribution of units within the "Bering Taiga" group is consistent (Fig. 12b). However, the "Brooks Foothills" in "Arctic Tundra" and the "Bering Sea Islands" in "Bering Tundra" tend to have a higher herbaceous cover than other units within groups do.

For the nonvascular (lichen and moss) component, the comparison between the Level 1 schemes shows a higher cover of nonvascular vegetation within the "Polar" scheme (Fig. 13a). The "Boreal" scheme shows an average coverage of 33.95% while that of the "Polar" scheme has a higher value of 41.32%. The "Boreal" scheme has an IQR of 15.24% to 40.11%, while that of the "Polar" scheme ranges from 23.41% to 56.99%. From north to south, the lichen/moss cover shows a slightly decreasing trend among the Level 2 groups and the ecoregion units (Fig. 13b). The mean values of lichen/moss cover in the "Arctic Tundra", "Bering Tundra" and "Bering Taiga" are about 47.14%, 36.90%, and 30.04% respectively. Specifically, the "Beaufort Coastal Plain" and "Brooks Range" show the highest coverages of lichen/moss compared to other units. Within the "Bering Tundra" and "Bering Taiga" groups, the nonvascular fractional cover also decreases gradually as the latitudes become lower.

We further compared our outputs with existing fractional vegetation cover products developed for the tundra. A scatter plot comparison between our field observations and the shrub cover circa 2000 (Beck et al., 2011) suggests that the 2000 shrub cover product overestimates the actual fractional cover of shrub in the North Slope (Fig. 14a). Compared to our field observations of fractional cover collected in the North Slope, the PFT maps circa 2015 (Macander et al., 2017) show an overestimation of shrub cover and an underestimation of lichen/moss cover, while the fractional cover values of herbaceous species (sedge/grass) are relatively comparable (Fig. 14b).

The comparison between our maps and the existing products using approximately 20,000 randomly selected pixels in the North Slope (Fig. 15) indicates similar patterns to those observed in comparing other products to field data directly. Fractional cover values of woody component (shrub) in both products are higher than the estimations in our results (Fig. 15a–b). Specifically, the majority of values were identified as 100% or 0% in Beck et al. (2011) in the North Slope. The fractional cover values of herbaceous species (sedge/grass) are comparable between our result and the product developed by Macander et al. (2017), ranging from about 20% to 75% (Fig. 15c). However, the coverage values of nonvascular component (lichen/moss) are much higher in our result when compared to those in the PFT product (Fig. 15d). The PFT product suggests that the nonvascular species including lichen and moss have a general coverage of 0%–25% in the North Slope, while our map indicates that lichen/moss can cover from 0% to 80%, mostly concentrated between 10% and 50% (Fig. 15d).

5. Discussion

Woody species in Alaskan tundra usually have higher surface reflectance in the NIR to SWIR spectrum but lower reflectance in the visible spectral regions compared to herbaceous species such as sedge and grass (Buchhorn et al., 2013; Strauss et al., 2012). Previous studies have demonstrated the importance of multi-spectral bands and NDVI in estimating the fractional coverage of shrub (Kushida et al., 2009; Selkowitz, 2010; Vierling et al., 1997). Multi-seasonal information and middle-infrared portion of the spectrum also contribute strongly to the accuracy of shrub cover prediction (Selkowitz, 2010). Both woody and herbaceous models demonstrate the importance of pre-growing season spectral information in distinguishing the woody and herbaceous components. This can be explained by their different phenological stages (Shaver and Kummerow, 1991). The in situ measurements of surface reflectance have shown that the lichen/moss component has different spectrum patterns when compared to woody or herbaceous species (Buchhorn et al., 2013; Huemmrich et al., 2013; Strauss et al., 2012). Our modeling result suggests that spectral indices integrating these bands in the post-growing season are effective in separating lichen/moss from woody and herbaceous components. This is likely to be driven by the exposure of spectral signals by lichen/moss due to the senescence of vascular species in the tundra during September.

In addition to spectral bands provided by 30-m Landsat imagery,

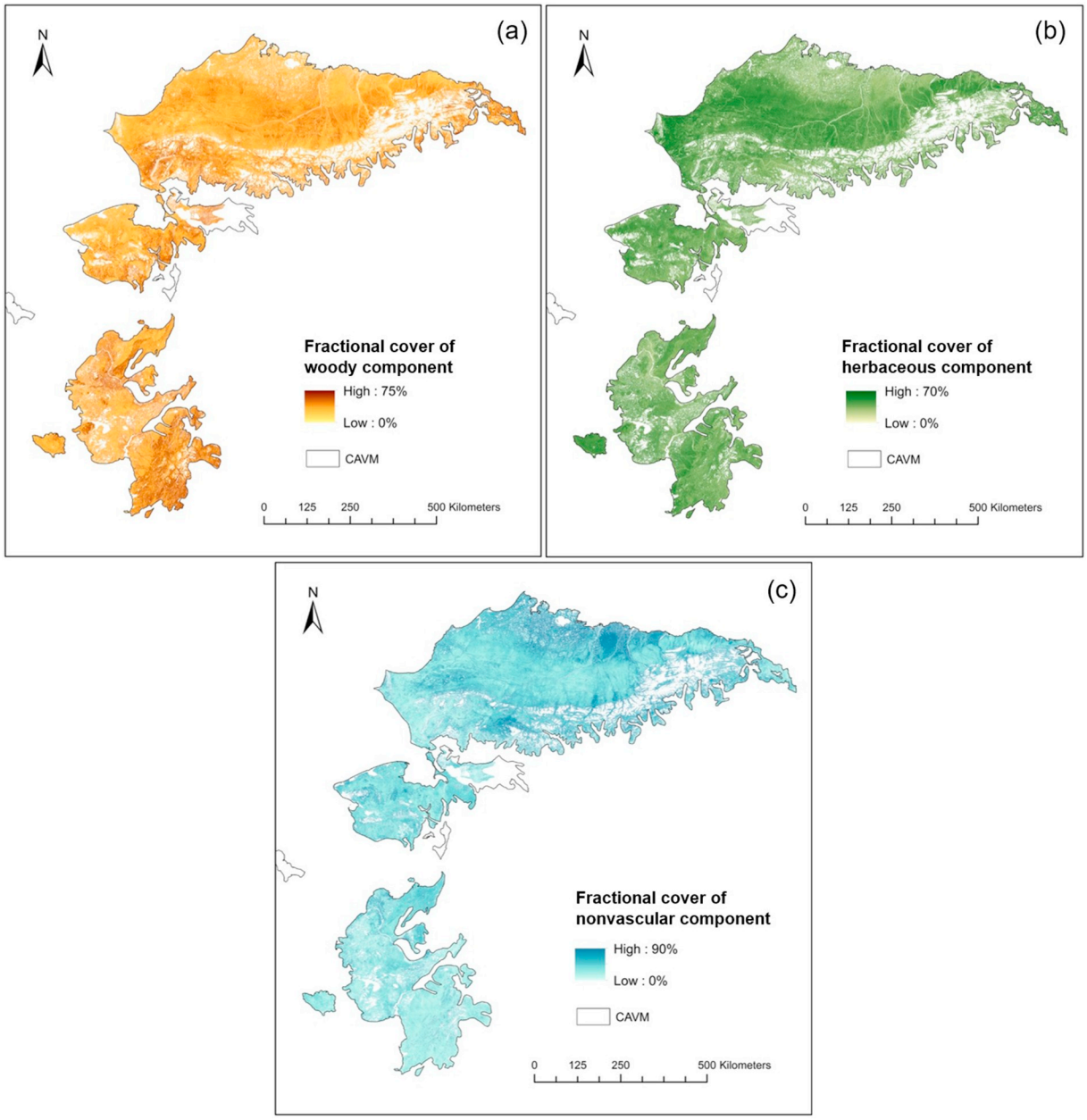

Fig. 9. Fractional cover of three major fuel type components across Alaskan tundra: (a) woody, (b) herbaceous, and (c) nonvascular components.

existing research has suggested that higher spatial resolution and red-edge (RE) spectral bands have the potential to improve fractional vegetation mapping efforts in the tundra (Davidson et al., 2016; Selkowitz, 2010; Stow et al., 1993). The launch of Sentinel-2 Multi-Spectral Instrument incorporating three RE bands provides the opportunity to improve the estimation accuracy of surface vegetation distribution at a broad spatial scale.

Developed only using spectral signatures, our mapping results also show effectiveness in representing the fuel component distribution across ecoregions with different bioclimatic conditions. The "Boreal" ecoregion scheme shows a higher cover of the woody component but a lower cover of the nonvascular component than the "Polar" ecoregion scheme in general. Mostly located in interior Alaska with a dry continental climate, ecoregions in the "Boreal" scheme tend to be dominated by shrubs and even boreal forests in these mountainous regions. Within the "Polar" scheme, the fractional cover of fuel components identified in this study also corresponds to the bioclimatic environment based on expert knowledge (Gallant et al., 1995; Nowacki et al., 2003). The low fractional cover values of the woody component in the Beaufort Coastal Plain and Brooks Foothills ecoregions are likely to be driven by their polar climate and poor soil drainage conditions. With higher summer temperature and more annual precipitation then other tundra areas, ecoregions as part of the "Bering Taiga" group (Nulato Hills, Yukon-Kuskokwim Delta and Ahklun Mountains) are covered with more woody fuels such as dwarf or tall scrub communities with wet graminoid species dominating in some regions, which is also evident in our maps.

Although our accuracy assessment shows strong predictive capability for fractional fuel mapping in Alaskan tundra, uncertainties still exist in our modeling and mapping results due to the limited spatial coverage of field observations, partially caused by the difficulty of obtaining field observations in the tundra. Regions with no available field data such as the Southwest Alaska and the northern North Slope could have higher uncertainties in our fractional cover maps. The mismatch of spatial resolutions between our 10 × 10 m field plots and the 30 × 30 m Landsat 8 pixels could also introduce errors in the

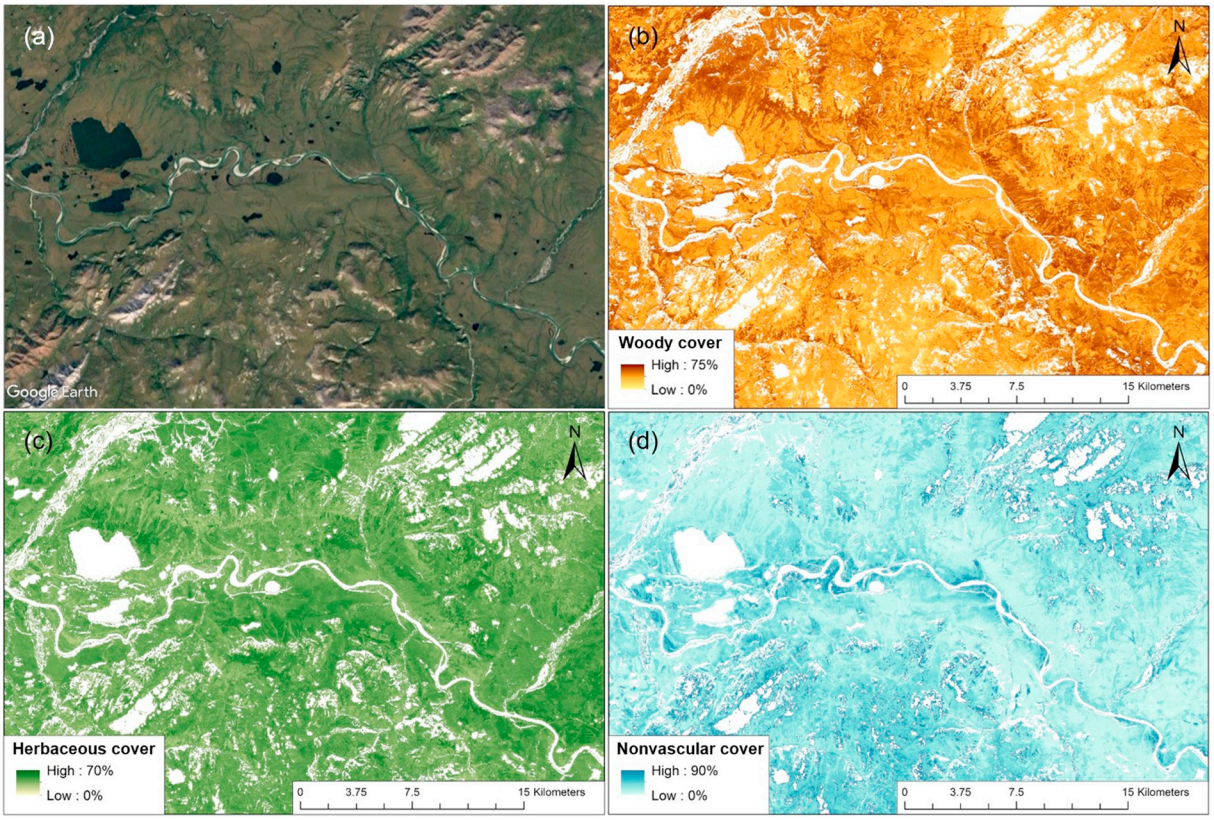

Fig. 10. Examples of fractional cover distribution in a tundra region near Lake Narvakrak in the Noatak River National Preserve: (a) VHR image from Google Earth; (b) fractional cover of woody component; (b) fractional cover of herbaceous component; (d) fractional cover of nonvascular component.

modeling and validation processes. During field campaigns, we have made our efforts on establishing sample plots in areas with visibly homogeneous distributions of vegetation species. However, it is possible that the actual vegetation coverages across one Landsat pixel may not be fully represented by the smaller than pixel field plots. Since the impacts of sample plot size on modeling and validation of fractional coverages is still unknown, future studies can elaborate on this and provide insights.

In addition, our results largely rely on the quality of the seasonal mosaics developed across the entire study area. First, maintaining the

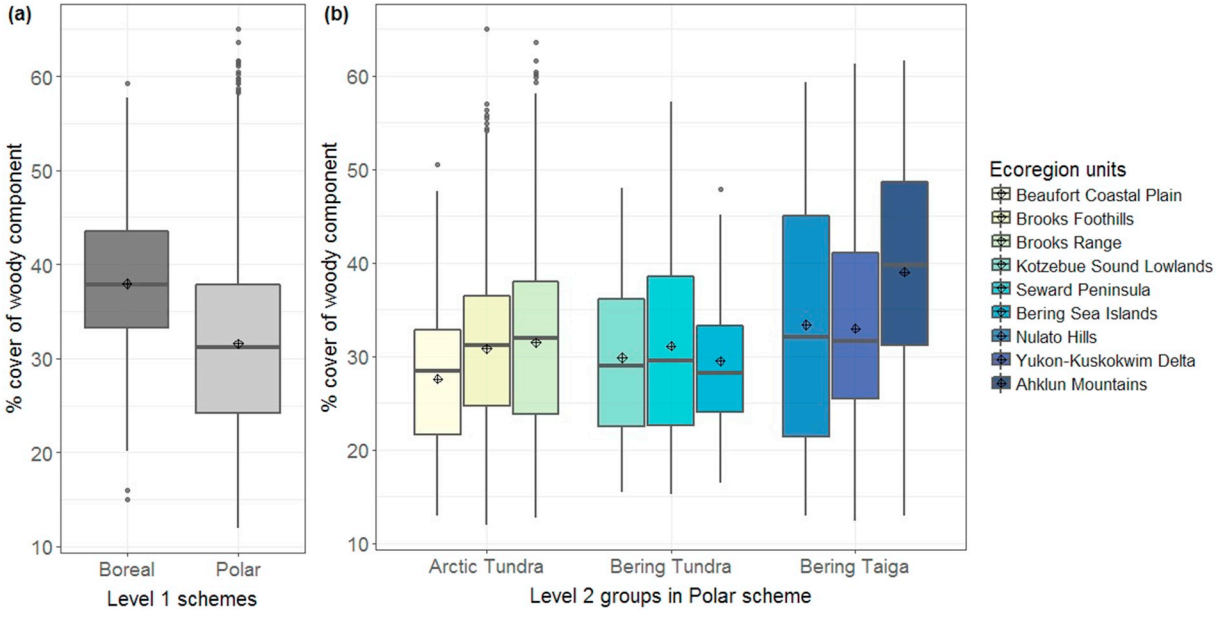

Fig. 11. Boxplots of woody component cover against ecoregions in Alaskan tundra: (a) woody component cover by Level 1 scheme; (b) woody component cover by Level 2 ecoregion groups in the "Polar" scheme (ecoregion units are colored from light yellow to dark blue based on the latitude from north to south). Shrub coverage increases gradually among all the Level 2 groups and the ecoregion units, from north to south (b). (For interpretation of the references to colour in this figure legend, the reader is referred to the web version of this article.)

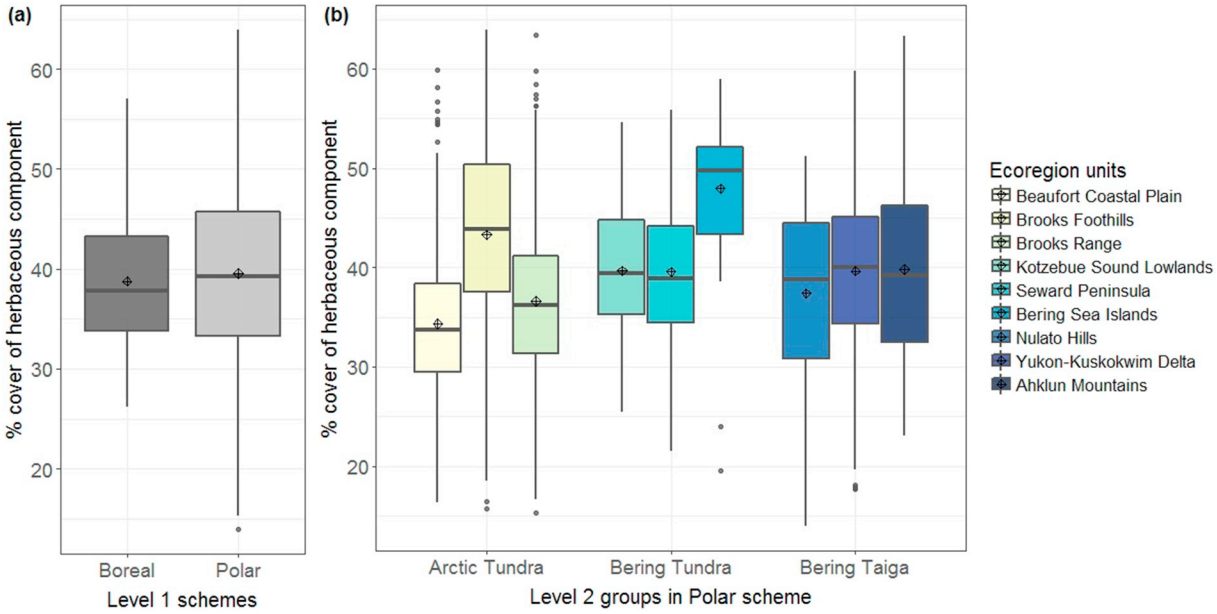

Fig. 12. Boxplots of herbaceous component cover against ecoregions in Alaskan tundra: (a) herbaceous component cover by Level 1 scheme; (b) herbaceous component cover by Level 2 ecoregion groups in the "Polar" scheme (ecoregion units are colored from light yellow to dark blue based on the latitude from north to south). Herbaceous cover values among Level 2 groups are generally comparable, with relative higher values in the "Brooks Foothills" and "Bering Sea Islands" units (b). (For interpretation of the references to colour in this figure legend, the reader is referred to the web version of this article.)

spatial consistency of these mosaics in Alaskan tundra is hindered by the pervasive cloud coverage and incomplete masking of cloud and cloud shadow pixels in the Landsat data. Although the CFMask algorithm delineates the major regions of cloud and shadow, it fails to identify all cloud- and shadow-impacted pixels. Second, matching multiple phenological stages of vegetation across different regions is challenging because of the differences in illumination properties and vegetation growing states under different climatic conditions (Muller et al., 1999; Selkowitz, 2010). Therefore, in order to maintain spatially and temporally consistent mosaics, we adopted the MVC method based on NDVI values with carefully defined growing periods using multi-year Landsat imagery.

It is also worth mentioning that the mismatches between our results and existing products (Section 4.3) can be caused by the differences in the cover definition and field sampling strategy. Beck et al. (2011) defined two shrub types – tall (> 1 m) and short – and mapped the total and tall shrub coverages. Here we chose the total shrub cover for comparison, which can explain why our estimates are lower. Macander et al. (2017) developed the fractional distribution maps of detailed PFTs. We used their integrated coverages of total shrubs, total herbaceous and top nonvascular plants for comparison, which can lead to the differences in our result comparisons. In addition, instead of

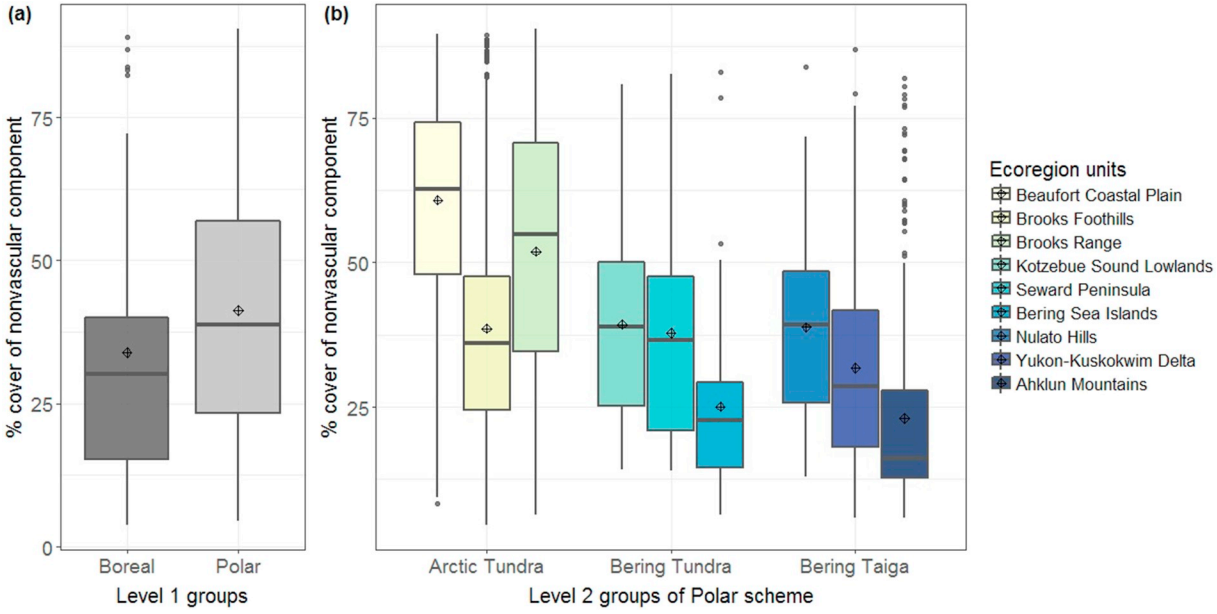

Fig. 13. Boxplots of nonvascular component cover against ecoregions in Alaskan tundra: (a) nonvascular component cover by Level 1 scheme; (b) nonvascular component cover by Level 2 ecoregion groups in the "Polar" scheme (ecoregion units are colored from light yellow to dark blue based on the latitude from north to south). Nonvascular coverage shows a decreasing trend among the Level 2 groups and the ecoregion units from north to south (b). (For interpretation of the references to colour in this figure legend, the reader is referred to the web version of this article.)

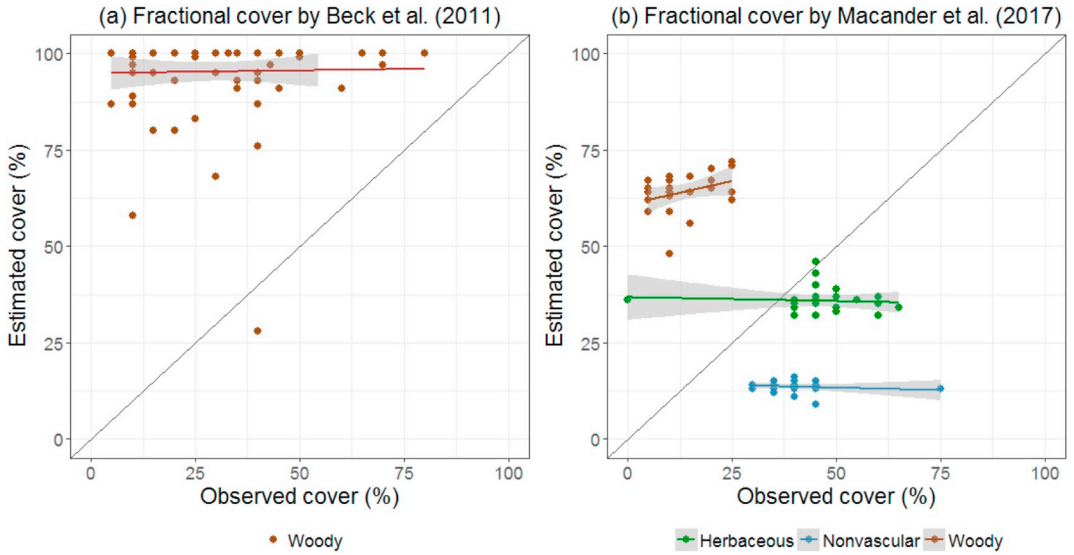

Fig. 14. Scatter plots comparing our field observations and estimations from other products: (a) 2000 shrub cover (Beck et al., 2011); (b) PFT products (Macander et al., 2017). Compared to our field observations, the PFT product (Macander et al., 2017) tends to overestimate the shrub cover, but underestimate the lichen/moss cover. The fractional cover of herbaceous species (sedge/grass) is relatively comparable.

collecting field measurements, Beck et al. (2011) extracted sample data by aggregating classified pixels from VHR imagery for training their regression algorithm, which could lead to the overestimation the actual shrub coverage in their mapping output. Moreover, Macander et al. (2017) collected field data from sites widely distributed across the North Slope, while our field data had no coverage within the Beaufort

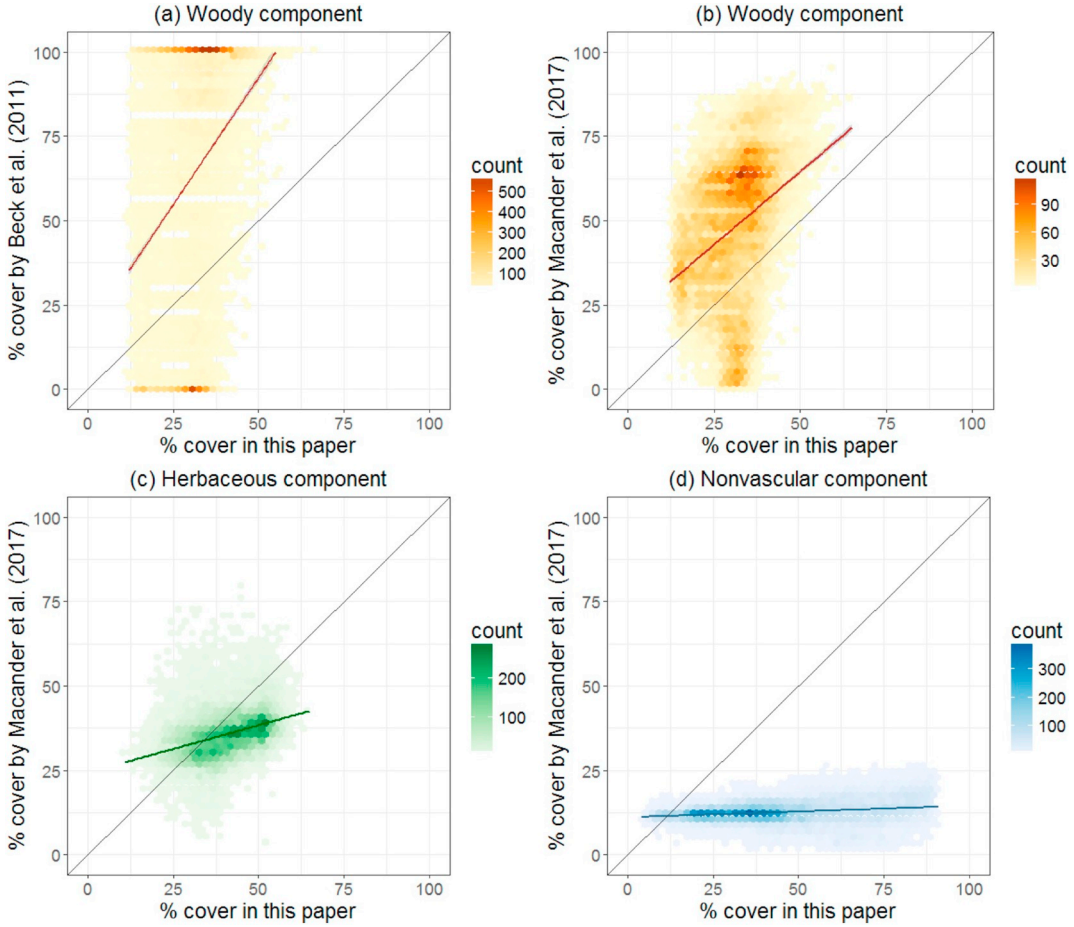

Fig. 15. Density plots comparing our results and estimations from existing products: (a) woody component cover circa 2000 by Beck et al. (2011); (b) woody component cover circa 2015 by Macander et al. (2017); (c) herbaceous component cover circa 2015 by Macander et al. (2017); (d) nonvascular component cover circa 2015 by Macander et al. (2017). Fractional cover values of woody component in both products are higher than the estimations in our results. Nonvascular component tends to have much higher coverage in our result than in the PFT product.

Coastal Plain ecoregion and only limited sites in the Brooks Foothills. This could explain the differences in the estimated cover of the non-vascular component in those regions between our result and that of Macander et al. (2017).

6. Conclusions

In this study, we deliver the first fractional cover maps of major fuel type components across Alaskan tundra circa 2015. We map the spatial distributions of woody, herbaceous and nonvascular components in this highly heterogeneous landscape. Although our field observations are comparatively limited in quantity and spatial coverage, our findings are broadly consistent with expected distribution according to bioclimatological conditions.

We present a method of using multi-spectral and multi-seasonal observations in the differentiation of fuel components. Our results show that this combination offers strong predictability from moderate resolution data and thus is critical for mapping efforts at a broad spatial scale. Our method can be adopted in monitoring other vegetation properties such as vegetation dominance and biomass.

In addition, the long-term archive of moderate resolution data in Alaska offers an opportunity to examine the fuel composition change in Alaskan tundra as a result of both climate change and fire occurrence. The outputs and spectral indicators identified in this paper can assist long-term monitoring of fuel type components in the tundra. These fuel maps and their periodic updates can create a strong basis for enhancing modeling capabilities for both assessing fire behavior and post-fire ecological impacts.

Acknowledgements

This work was supported by the NASA Terrestrial Ecology program grant NNX15AT79A. The authors would like to thank Dr. Nancy French from Michigan Technological Research Institute, Qing Ying and Lei Ma from the University of Maryland for their support and discussions.

References

Alaska Department of Fish and Game, 2006. Our Wealth Maintained: A Strategy for Conserving Alaska's Diverse Wildlife and Fish Resources. pp. 1–25.

Anderson, H.E., 1982. Fire Behavior Fuel Model Descriptions B1–B7.

Baig, M.H.A., Zhang, L., Shuai, T., Tong, Q., 2014. Derivation of a tasselled cap transformation based on Landsat 8 at-satellite reflectance. Remote Sens. Lett. 5, 423–431. https://doi.org/10.1080/2150704X.2014.915434.

Beamish, A., Coops, N., Chabrillat, S., Heim, B., 2017. A phenological approach to spectral differentiation of low-arctic tundra vegetation communities, north slope, Alaska. Remote Sens. 9, 1200. https://doi.org/10.3390/rs9111200.

Beck, P.S.A., Horning, N., Goetz, S.J., Loranty, M.M., Tape, K.D., 2011. Shrub cover on the north slope of Alaska: a circa 2000 baseline map. Arct. Antarct. Alp. Res. 43, 355–363. https://doi.org/10.1657/1938-4246-43.3.355.

Berner, L.T., Jantz, P., Tape, K.D., Goetz, S., 2018. Tundra plant aboveground biomass and shrub dominance mapped across the north slope of Alaska. Environ. Res. Lett. 13, 035002. https://doi.org/10.1088/1748-9326/aaaa9a.

Bhatt, U.S., Walker, D.A., Raynolds, M.K., Bieniek, P.A., Epstein, H.E., Comiso, J.C., Pinzon, J.E., Tucker, C.J., Polyakov, I.V., 2013. Recent declines in warming and vegetation greening trends over pan-arctic tundra. Remote Sens. 5, 4229–4254. https://doi.org/10.3390/rs5094229.

Bourgeau-Chavez, L.L., Kasischke, E.S., Riordan, K., Brunzell, S., Nolan, M., Hyer, E., Slawski, J., Medvecz, M., Walters, T., Ames, S., 2007. Remote monitoring of spatial and temporal surface soil moisture in fire disturbed boreal forest ecosystems with ERS SAR imagery. Int. J. Remote Sens. 28, 2133–2162. https://doi.org/10.1080/01431160600976061.

Bourgeau-Chavez, L.L., Leblon, B., Charbonneau, F., Buckley, J.R., 2013. Evaluation of polarimetric Radarsat-2 SAR data for development of soil moisture retrieval algorithms over a chronosequence of black spruce boreal forests. Remote Sens. Environ. 132, 71–85. https://doi.org/10.1016/j.rse.2013.01.006.

Breiman, L., 2001. Random forests. Mach. Learn. 45, 5–32.

Breiman, L., 2002. Manual on setting up, using, and understanding random forests v3. 1. Tech. Report, http//oz.berkeley.edu/users/breiman, Stat. Dep. Univ. Calif. Berkeley, … 29. doi:https://doi.org/10.2776/85168.

Buchhorn, M., Walker, D.A., Heim, B., Raynolds, M.K., Epstein, H.E., Schwieder, M., 2013. Ground-based hyperspectral characterization of Alaska tundra vegetation along environmental gradients. Remote Sens. 5, 3971–4005. https://doi.org/10.3390/rs5083971.

Carroll, M.L., Wooten, M.R., Dimiceli, C., Sohlberg, R.A., Townshend, J.R.G., 2016. ABoVE: Surface Water Extent. Boreal and Tundra Regions, North America, pp. 1991–2011. https://doi.org/10.3334/ornldaac/1324.

Chopping, M., Su, L., Rango, A., Martonchik, J.V., Peters, D.P.C., Laliberte, A., 2008. Remote sensing of woody shrub cover in desert grasslands using MISR with a geometric-optical canopy reflectance model. Remote Sens. Environ. 112, 19–34. https://doi.org/10.1016/j.rse.2006.04.023.

Chopping, M., North, M., Chen, J., Schaaf, C.B., Blair, J.B., Martonchik, J.V., Bull, M.A., 2012. Forest canopy cover and height from MISR in topographically complex southwestern US landscapes assessed with high quality reference data. IEEE J. Sel. Top. Appl. Earth Obs. Remote Sens. 5, 44–58. https://doi.org/10.1109/JSTARS.2012.2184270.

Davidson, S., Santos, M., Sloan, V., Watts, J., Phoenix, G., Oechel, W., Zona, D., 2016. Mapping arctic tundra vegetation communities using field spectroscopy and multispectral satellite data in north Alaska, USA. Remote Sens. 8, 978. https://doi.org/10.3390/rs8120978.

Dyrness, C.T., Norum, R.A., 1983. The effects of experimental fires on black spruce forest floors in interior Alaska. Can. J. For. Res. 13, 879–893. https://doi.org/10.1139/x83-118.

French, N.H.F., Jenkins, L.K., Loboda, T.V., Flannigan, M., Jandt, R., Bourgeau-Chavez, L.L., Whitley, M., 2015. Fire in arctic tundra of Alaska: past fire activity, future fire potential, and significance for land management and ecology. Int. J. Wildland Fire 24, 1045–1061. https://doi.org/10.1071/WF14167.

French, N.H.F., Whitley, M.A., Jenkins, L.K., 2016. Fire disturbance effects on land surface albedo in Alaskan tundra. J. Geophys. Res. Biogeosci. 121, 841–854. https://doi.org/10.1002/2015JG003177.

Frost, G.V., Epstein, H.E., Walker, D.A., 2014. Regional and landscape-scale variability of Landsat-observed vegetation dynamics in northwest Siberian tundra. Environ. Res. Lett. 9, 25004.

Gallant, A.L., Binnian, E.F., Omernik, J.M., Shasby, M.B., 1995. Ecoregions of Alaska - U.S. Geological Survey Professional Paper 1567 73. (doi:0160482909r0607010010).

Gao, B., 1996. NDWI – a normalized difference water index for remote sensing of vegetation liquid water from space. Remote Sens. Environ. 58, 257. https://doi.org/10.1016/S0034-4257(96)00067-3.

García, M.J.L., Caselles, V., 1991. Mapping burns and natural reforestation using thematic mapper data. Geocarto Int 6, 31–37. https://doi.org/10.1080/10106049109354290.

Gessner, U., Machwitz, M., Conrad, C., Dech, S., 2013. Estimating the fractional cover of growth forms and bare surface in savannas. A multi-resolution approach based on regression tree ensembles. Remote Sens. Environ. 129, 90–102. https://doi.org/10.1016/j.rse.2012.10.026.

Guan, K., Wood, E.F., Caylor, K.K., 2012. Multi-sensor derivation of regional vegetation fractional cover in Africa. Remote Sens. Environ. 124, 653–665. https://doi.org/10.1016/j.rse.2012.06.005.

Hansen, M.C.C., Potapov, P.V., Moore, R., Hancher, M., Turubanova, S.A. a, Tyukavina, A., Thau, D., Stehman, S.V.V., Goetz, S.J.J., Loveland, T.R.R., Kommareddy, A., Egorov, A., Chini, L., Justice, C.O.O., Townshend, J.R.G.R.G., Patapov, P.V., Moore, R., Hancher, M., Turubanova, S.A. a, Tyukavina, A., Thau, D., Stehman, S.V.V., Goetz, S.J.J., Loveland, T.R.R., Kommaredy, A., Egorov, A., Chini, L., Justice, C.O.O., Townshend, J.R.G.R.G., 2013. High-resolution global maps of 21st-century forest cover change. Science 342, 850–854. https://doi.org/10.1126/science.1244693. 80-.

Higuera, P.E., Chipman, M.L., Barnes, J.L., Urban, M.A., Hu, F.S., 2011. Variability of tundra fire regimes in Arctic Alaska: millennial-scale patterns and ecological implications. Ecol. Appl. 21, 3211–3226. https://doi.org/10.1890/11-0387.1.

Hirsch, K.G., 1996. Canadian Forest Fire Behavior Prediction (FBP) System: User's Guide, Special Report 7. Northern Forestry Centre, Edmonton.

Holben, B.N., 1986. Characteristics of maximum-value composite images from temporal AVHRR data. Int. J. Remote Sens. 7, 1417–1434. https://doi.org/10.1080/01431160600948945.

Hu, F.S., Higuera, P.E., Duffy, P., Chipman, M.L., Rocha, A.V., Young, A.M., Kelly, R., Dietze, M.C., 2015. Arctic tundra fires: natural variability and responses to climate change. Front. Ecol. Environ. https://doi.org/10.1890/150063.

Huemmrich, K.F., Gamon, J.A., Tweedie, C.E., Campbell, P.K.E., Landis, D.R., Middleton, E.M., 2013. Arctic tundra vegetation functional types based on photosynthetic physiology and optical properties. IEEE J. Sel. Top. Appl. Earth Obs. Remote Sens. 6, 265–275. https://doi.org/10.1109/JSTARS.2013.2253446.

Innes, R.J., 2013. Fire Regimes of Alaskan Tundra Communities, Fire Effects Information System, [Online].

Jones, B.M., Grosse, G., Arp, C.D., Miller, E., Liu, L., Hayes, D.J., Larsen, C.F., 2015. Recent Arctic tundra fire initiates widespread thermokarst development. Sci. Rep. 5, 15865. https://doi.org/10.1038/srep15865.

Kasischke, E.S., Hoy, E.E., 2012. Controls on carbon consumption during Alaskan wildland fires. Glob. Chang. Biol. 18, 685–699. https://doi.org/10.1111/j.1365-2486.2011.02573.x.

Kushida, K., Kim, Y., Tsuyuzaki, S., Fukuda, M., 2009. Spectral vegetation indices for estimating shrub cover, green phytomass and leaf turnover in a sedge-shrub tundra. Int. J. Remote Sens. 30, 1651–1658. https://doi.org/10.1080/01431160802502632.

Lara, M.J., Nitze, I., Grosse, G., McGuire, A.D., 2018. Tundra landform and vegetation productivity trend maps for the arctic coastal plain of northern Alaska. Sci. Data 5, 180058.

Liu, X., Liu, H., Qiu, S., Wu, X., Tian, Y., Hao, Q., 2017. An improved estimation of regional fractional woody/herbaceous cover using combined satellite data and high-quality training samples. Remote Sens. 9. https://doi.org/10.3390/rs9010032.

Loboda, T.V., French, N.H.F., Hight-Harf, C., Jenkins, L., Miller, M.E., 2013. Mapping fire extent and burn severity in Alaskan tussock tundra: an analysis of the spectral response of tundra vegetation to wildland fire. Remote Sens. Environ. 134, 194–209. https://doi.org/10.1016/j.rse.2013.03.003.

Loboda, T.V., Hall, J.V., Hall, A.H., Shevade, V.S., 2017. ABoVE: cumulative annual burned area. In: Circumpolar High Northern Latitudes, pp. 2001–2015. https://doi.org/10.3334/ornldaac/1526.

Louppe, G., Wehenkel, L., Sutera, A., Geurts, P., 2013. Understanding variable importances in forests of randomized trees. Adv. Neural Inf. Proces. Syst. 26, 431–439 (doi:NIPS2013_4928).

Ma, L., Zhou, Y., Chen, J., Cao, X., Chen, X., 2015. Estimation of fractional vegetation cover in semiarid areas by integrating endmember reflectance purification into nonlinear spectral mixture analysis. IEEE Geosci. Remote Sens. Lett. 12, 1175–1179. https://doi.org/10.1109/LGRS.2014.2385816.

Macander, M.J., Frost, G.V., Nelson, P.R., Swingley, C.S., 2017. Regional quantitative cover mapping of tundra plant functional types in Arctic Alaska. Remote Sens. 9, 1–26. https://doi.org/10.3390/rs9101024.

Mack, M.C., Bret-Harte, M.S., Hollingsworth, T.N., Jandt, R.R., Schuur, E.A.G., Shaver, G.R., Verbyla, D.L., 2011. Carbon loss from an unprecedented Arctic tundra wildfire. Nature 475, 489–492. https://doi.org/10.1038/nature10283.

Marino, E., Ranz, P., Tomé, J.L., Noriega, M., Esteban, J., Madrigal, J., 2016. Generation of high-resolution fuel model maps from discrete airborne laser scanner and Landsat-8 OLI: a low-cost and highly updated methodology for large areas. Remote Sens. Environ. 187, 267–280. https://doi.org/10.1016/j.rse.2016.10.020.

Masrur, A., Petrov, A.N., DeGroote, J., 2018. Circumpolar spatio-temporal patterns and contributing climatic factors of wildfire activity in the Arctic tundra from 2001–2015. Environ. Res. Lett. 13. https://doi.org/10.1088/1748-9326/aa9a76.

McFeeters, S.K., 1996. The use of the normalized difference water index (NDWI) in the delineation of open water features. Int. J. Remote Sens. 17, 1425–1432.

McManus, K.M., Morton, D.C., Masek, J.G., Wang, D., Sexton, J.O., Nagol, J.R., Ropars, P., Boudreau, S., 2012. Satellite-based evidence for shrub and graminoid tundra expansion in northern Quebec from 1986 to 2010. Glob. Chang. Biol. 18, 2313–2323. https://doi.org/10.1111/j.1365-2486.2012.02708.x.

Mu, X., Song, W., Gao, Z., McVicar, T.R., Donohue, R.J., Yan, G., 2018. Fractional vegetation cover estimation by using multi-angle vegetation index. Remote Sens. Environ. 216, 44–56. https://doi.org/10.1016/j.rse.2018.06.022.

Muller, S.V., Racoviteanu, A.E., Walker, D.A., 1999. Landsat MSS-derived land-cover map of northern Alaska: extrapolation methods and a comparison with photo-interpreted and AVHRR-derived maps. Int. J. Remote Sens. 20, 2921–2946.

Nowacki, G.J., Spencer, P., Fleming, M., Brock, T., Jorgenson, T., 2003. Unified ecoregions of Alaska: 2001. Open-File Report. https://doi.org/10.3133/ofr2002297.

Okin, G.S., 2007. Relative spectral mixture analysis — a multitemporal index of total vegetation cover. Remote Sens. Environ. 106, 467–479. https://doi.org/10.1016/j.rse.2006.09.018.

Olthof, I., Fraser, R.H., 2007. Mapping northern land cover fractions using Landsat ETM +. Remote Sens. Environ. 107, 496–509. https://doi.org/10.1016/j.rse.2006.10.009.

Ottmar, R.D., Sandberg, D.V., Riccardi, C.L., Prichard, S.J., 2007. An overview of the fuel characteristic classification system — quantifying, classifying, and creating fuelbeds for resource planningThis article is one of a selection of papers published in the special forum on the fuel characteristic classification Syste. Can. J. For. Res. 37, 2383–2393. https://doi.org/10.1139/X07-077.

Pearson, R.G., Phillips, S.J., Loranty, M.M., Beck, P.S.A., Damoulas, T., Knight, S.J., Goetz, S.J., 2013. Shifts in Arctic vegetation and associated feedbacks under climate change. Nat. Clim. Chang. 3, 673–677. https://doi.org/10.1038/nclimate1858.

Potapov, P., Hansen, M.C., Stehman, S.V., Loveland, T.R., Pittman, K., 2008. Combining MODIS and Landsat imagery to estimate and map boreal forest cover loss. Remote Sens. Environ. 112, 3708–3719. https://doi.org/10.1016/J.RSE.2008.05.006.

Pyne, S.J., Andrews, P.L., Laven, R.D., 1996. Introduction to Wildland Fire, Second Edi. John Wiley & Sons, Inc.

Racine, C., Jandt, R., Meyers, C., Dennis, J., 2004. Tundra fire and vegetation change along a hillslope on the Seward peninsula, Alaska, U.S.a. Arctic. Antarct. Alp. Res. 36, 1–10. https://doi.org/10.1657/1523-0430(2004)036[0001:TFAVCA]2.0.CO;2.

Raynolds, M.K., Comiso, J.C., Walker, D.A., Verbyla, D., 2008. Relationship between satellite-derived land surface temperatures, arctic vegetation types, and NDVI. Remote Sens. Environ. 112, 1884–1894. https://doi.org/10.1016/j.rse.2007.09.008.

Rocha, A.V., Loranty, M.M., Higuera, P.E., Mack, M.C., Hu, F.S., Jones, B.M., Breen, A.L., Rastetter, E.B., Goetz, S.J., Shaver, G.R., 2012. The footprint of Alaskan tundra fires during the past half-century: implications for surface properties and radiative forcing. Environ. Res. Lett. 7, 044039. https://doi.org/10.1088/1748-9326/7/4/044039.

Roy, D.P., Ju, J., Kline, K., Scaramuzza, P.L., Kovalskyy, V., Hansen, M., Loveland, T.R., Vermote, E., Zhang, C., 2010. Web-enabled Landsat data (WELD): Landsat ETM+ composited mosaics of the conterminous United States. Remote Sens. Environ. 114, 35–49. https://doi.org/10.1016/j.rse.2009.08.011.

Scott, J.H., Burgan, R.E., 2005. Standard Fire Behavior Fuel Models: A Comprehensive Set for Use With Rothermel's Surface Fire Spread Model. https://doi.org/10.2737/RMRS-GTR-153.

Selkowitz, D.J., 2010. A comparison of multi-spectral, multi-angular, and multi-temporal remote sensing datasets for fractional shrub canopy mapping in Arctic Alaska. Remote Sens. Environ. 114, 1338–1352. https://doi.org/10.1016/j.rse.2010.01.012.

Shaver, G.R., Kummerow, J., 1991. Phenology, resource allocation, and growth of arctic vascular plants. In: Arctic Ecosystems in a Changing Climate. Elsevier, pp. 193–211.

Somers, B., Asner, G.P., Tits, L., Coppin, P., 2011. Endmember variability in spectral mixture analysis: a review. Remote Sens. Environ. 115, 1603–1616. https://doi.org/10.1016/j.rse.2011.03.003.

Stow, D.A., Burns, B.H., Hope, A.S., 1993. Spectral, spatial and temporal characteristics of Arctic tundra reflectance. Int. J. Remote Sens. 14, 2445–2462. https://doi.org/10.1080/01431169308904285.

Stow, D.A., Hope, A., McGuire, D., Verbyla, D., Gamon, J., Huemmrich, F., Houston, S., Racine, C., Sturm, M., Tape, K., Hinzman, L., Yoshikawa, K., Tweedie, C., Noyle, B., Silapaswan, C., Douglas, D., Griffith, B., Jia, G., Epstein, H., Walker, D., Daeschner, S., Petersen, A., Zhou, L., Myneni, R., 2004. Remote sensing of vegetation and land-cover change in Arctic tundra ecosystems. Remote Sens. Environ. 89, 281–308. https://doi.org/10.1016/j.rse.2003.10.018.

Strauss, J., Ulrich, M., Buchhorn, M., 2012. Expeditions to Permafrost 2012: "Alaskan North Slope/Itkillik", "Thermokarst in Central Yakutia", "EyeSight-NAAT-Alaska.".

Sylvester, T.W., Wein, R.W., 1981. Fuel characteristics of arctic plant species and simulated plant community flammability by Rothermel's model. Can. J. Bot. 59, 898–907. https://doi.org/10.1139/b81-125.

Tucker, C.J., 1979. Red and photographic infrared linear combinations for monitoring vegetation. Remote Sens. Environ. 8, 127–150. https://doi.org/10.1016/0034-4257(79)90013-0.

Vermote, E., Justice, C., Claverie, M., Franch, B., 2016. Preliminary analysis of the performance of the Landsat 8/OLI land surface reflectance product. Remote Sens. Environ. 185, 46–56. https://doi.org/10.1016/j.rse.2016.04.008.

Viereck, L.A., 1979. Preliminary Results of Experimental Fires in the Black Spruce Type of Interior Alaska. Dept. of Agriculture, Forest Service, Pacific Northwest Forest and Range Experiment Station.

Viereck, L.A., Dyrness, C.T., Batten, A.R., Wenzlick, K.J., 1992. The Alaska vegetation classification. USDA Gen. Tech. Rep. 284.

Vierling, L.A., Deering, D.W., Eck, T.F., 1997. Differences in arctic tundra vegetation type and phenology as seen using bidirectional radiometry in the early growing season. Remote Sens. Environ. 60, 71–82. https://doi.org/10.1016/S0034-4257(96)00139-3.

Walker, D.A., Raynolds, M.K., Daniëls, F.J.A., Einarsson, E., Elvebakk, A., Gould, W.A., Katenin, A.E., Kholod, S.S., Markon, C.J., Melnikov, E.S., Moskalenko, N.G., Talbot, S.S., Yurtsev, B.A., Team, the other members of the C, 2005. The circumpolar Arctic vegetation map. J. Veg. Sci. 16, 267–282. https://doi.org/10.1111/j.1654-1103.2005.tb02365.x.

Young, A.M., Higuera, P.E., Duffy, P.A., Hu, F.S., 2017. Climatic thresholds shape northern high-latitude fire regimes and imply vulnerability to future climate change. Ecography (Cop.) 40, 606–617. https://doi.org/10.1111/ecog.02205.

Zhu, Z., Wang, S., Woodcock, C.E., 2015. Improvement and expansion of the Fmask algorithm: cloud, cloud shadow, and snow detection for Landsats 4–7, 8, and Sentinel 2 images. Remote Sens. Environ. 159, 269–277. https://doi.org/10.1016/j.rse.2014.12.014.